Developing a Novel Clinically Representative Biofilm Based Gram-Negative Prosthetic Joint Infection Rat Hip Hemiarthroplasty Model

By

Mazen Mohamed Ibrahim Ibrahim

A Thesis Submitted to the Faculty of Medicine, University of Ottawa in Partial Fulfillment of the Requirements for the M.Sc. Degree in Microbiology and Immunology Specialization in Pathology and Experimental Medicine

Department of Biochemistry, Microbiology, and Immunology
Faculty of Medicine
University of Ottawa

ABSTRACT

Introduction: Gram-negative prosthetic joint infections (GN-PJI) present unique challenges in management due to their distinct pathogenesis of biofilm formation on implant surfaces. The purpose of this study is to establish a clinically representative GN-PJI model that can reliably recapitulate biofilm formation on titanium implant surface *in vivo*. I hypothesized that biofilm formation on an implant surface will affect its ability to osseointegrate. **Methods:** The model was developed using 3D-printed titanium hip implants, to replace the femoral head of male Sprague-Dawley rats using a posterior surgical approach. GN-PJI was induced using two bioluminescent *Pseudomonas aeruginosa* (PA) strains: a reference strain (PA14-*lux*) and a mutant strain that is defective in biofilm formation (*ΔflgK-lux*). Infection was assessed in real-time using the *in vivo imaging system* (IVIS) and Magnetic Resonance Imaging (MRI) and *in vitro* by quantifying bacterial loads on collected implants surface and in periprosthetic tissues as well as biofilm visualization using the Field emission scanning electron microscopy (FE-SEM). The implant stability, as an outcome, was directly assessed by quantifying the osseointegration *in vitro* using microCT scan, and indirectly assessed by identifying the gait pattern changes using DigiGait^{TM} system *in vivo*. **Results:** Bioluminescence detected by IVIS, was focused on the hip region, demonstrating localized-infection, with the ability of PA14-*lux* to persist in the model compared to *ΔflgK-lux* defective in biofilm formation. This was corroborated by MRI as the PA14-*lux* induced relatively larger implant-related abscesses. Biofilm formation at the bone-implant-interface induced by the PA14-*lux* was visualized using FE-SEM versus defective-biofilm formation by *ΔflgK-lux*. This could be quantitatively confirmed, by average viable-colony-count of the sonicated implants, $3.77x10^8$CFU/ml versus $3.65x10^3$CFU/ml for PA14-*lux* and *ΔflgK-lux*, respectively (p=0.0025; 95%CI: $-6.08x10^8$ to $-1.45x10^8$). This difference in the ability to persist in the model was reflected significantly on the implant osseointegration with a mean intersection surface $4.1x10^6\mu m^2 \pm 1.99x10^6$ for PA14-*lux* versus $6.44x10^6\mu m^2 \pm 2.53x10^6$ for *ΔflgK-lux* and $7.08x10^6\mu m^2 \pm 1.55x10^6$ for non-infected control (p=0.048). **Conclusions:** To date, the proposed *in vivo* biofilm-based model is the most clinically representative for GN-PJI since animals can bear weight on the implant and poor osseointegration correlates with biofilm formation. **Clinical Relevance:** The current model will allow for reliable testing of novel biofilm-targeting therapeutics.

ACKNOWLEDGEMENTS:

The work presented in this thesis could not have been completed without the help of numerous individuals. I would like to thank:

- **Drs. Thien-Fah Mah** and **Hesham Abdelbary**, for being outstanding supervisors.
- My TAC members, **Drs. Emilio Alarcon,** and **Juthaporn Cowan** for their guidance and critical analysis of my work.
- **Clayton Hall, Li Zhang** and **Caetanie Tchagang**, for all their help with the technical aspects of experiments that were completed in the lab.
- **Dr. Adam Paish** (and the **David Wayne Holdsworth Lab**, the University of Western Ontario), for their help with everything related to the creation of 3D-printed medical-grade titanium hip implants.
- **Dr. Kerstin Ure** and the animal behavior, physiology core, University of Ottawa, Faculty of Medicine, Ottawa, Canada, for their help in digiGait analysis.
- **Yun Liu** and the materials characterization core facility, centre for advanced materials research (camar), University of Ottawa, Ottawa, Canada for her help in scanning electron microscopy
- My friends at **BMIGSA**, for their support.
- Department of Surgery and Orthopedic Division for funding this research project through **Doctor Hans Uthoff scholarship** and the **Translational Research Grant**.

Finally, I would like to thank my family for their support throughout the entirety of my work.

Thank you.

LIST OF ABBREVIATIONS

TJA	Total Joint Arthroplasty
PJI	Prosthetic Joint Infection
GP	Gram-positive
GN	Gram-negative
PA	*Pseudomonas aeruginosa*
DAIR	Debridement, Antibiotics, and Implant Retention
EPSs	Extracellular Polymeric Substances
PIA	Polysaccharide Intercellular Adhesin
eDNA	extracellular DNA
sad	surface attachment defective
MBC	Minimal Bactericidal Concentration
LPS	Lipopolysaccharide
IVIS	*in vivo* imaging system
PVC	Polyvinylchloride
CV	crystal violet
LB	Luria-Bertani
TAE	Tris-acetate-EDTA
bla	beta lactamase
GmR	Gentamicin resistance
ALI	Air Liquid Interface
FE-SEM	Field emission scanning electron microscopy
MRI	Magnetic Resonance Imaging
ROI	region of interest
IS	Intersection surface
BIC	bone-to-implant contact
POD	Post-Operative Day

TABLE OF CONTENTS

ABSTRACT……ii
ACKNOWLEDGEMENTS……iii
LIST OF ABBREVIATIONS……iv
TABLE OF CONTENTS……v
LIST OF TABLES……vii
LIST OF FIGURES……viii
CHAPTER 1: INTRODUCTION……1
1.1 Prosthetic Joint Infection……1
1.1.1 Epidemiology……2
1.1.2 Economic Burden……2
1.1.3 Gram Negative Prosthetic Joint Infection……2
1.1.4 Treatment of PJI……3
1.2 Biofilm……5
1.2.1 Structure of Biofilm……5
1.2.2 Biofilm Development *in vitro*……6
1.2.3 *Pseudomonas aeruginosa* as a model organism to study GN-biofilm……7
1.2.4 Surface Attachment Deficient *sad* genes……8
1.3 Role of Bacterial Biofilms in Implant Related Infections……8
1.4 Prosthetic Joint Infection Animal Models……9
1.4.1 Model Animal Selection……9
1.4.2 Model Implant Selection……10
1.4.3 Model Organism (Pathogen) Selection……12
1.5 Outlook and Clinical Significance……13
CHAPTER 2: METHODS……14
2.1 Experimental Design……14
2.2 Model Organism……14
2.2.1 Determination of a Negative Control for *in vivo* Model……15
2.2.2 Construction of Bioluminescent PA Strains……18
2.2.3 Mini-Tn7 System……18
2.2.4 Plasmid DNA Purification……18

2.2.5 Diagnostic Restriction Enzyme Digestion……19
2.2.6 Constructing a bioluminescent PA strain utilizing Tn7 system……22
2.2.7 Characterization of the Constructed Strains……...24
2.3 Model System……26
2.3.1 Model Implant……27
2.3.2 Surgical Procedure……27
2.3.3 Bacterial Inoculum Preparation……30
2.3.4 Establishment of Biofilm-based GN-PJI……...30
2.4 Qualitative and Quantitative Assessment of PJI……31
2.4.1 Real-time Monitoring of PJI……...31
2.4.2 Magnetic Resonance Imaging (MRI)……31
2.4.3 DigiGait Analysis……...31
2.4.4 Bacterial Load Quantification……32
2.4.5 Testing Osseointegration Utilizing microCT Analysis……32
2.4.6 Field-Emission Scanning Electron Microscopy (FE-SEM) ……33
2.5 Statistical analysis……33
CHAPTER 3: RESULTS……34
3.1 Evaluating Systemic Response to GN-PJI……34
3.2 Evaluation of Biofilm Formation and Periprosthetic Tissue……35
3.2.1 Real-time Monitoring of PJI (*in vivo*) ……35
3.2.2 Bacterial Load (*in vitro*) ……37
3.2.3 MRI (*in vivo*) ……38
3.2.4 FE-SEM (*in vitro*) ……39
3.3 Evaluation of the Implant Stability and Function……...40
3.3.1 DigiGait Analysis (*in vivo*) ……40
3.3.2 Testing Osseointegration Utilizing microCT Analysis (*in vitro*) ...……41
CHAPTER 4: DISCUSSION……42
LIST OF REFERENCES……...48
CONTRIBUTION OF COLLABORATORS……68
CURRICULUM VITAE……69

LIST OF TABLES

Table1: Plasmids Utilized for mini-Tn7……. 18

Table 2: Diagnostic Digestion for mini-Tn7 delivery vector pUC18-mini-Tn7T-Gm-*lux*… 20

Table 3: Diagnostic Digestion for mini-Tn7 helper plasmid TNS2……..... 21

Table 4: List of Primers for Pair Primer Colony PCR……..... 23

Table 5: Ingredients for PCR……. 23

Table 6: PCR conditions……. 23

LIST OF FIGURES

Figure 1: Hip hemiarthroplasty implant reproduces the periprosthetic environment……. 11

Figure 2: Experiment Timeline……... 14

Figure 3: Determination of a Negative Control for *in vivo* Model……. 17

Figure 4: Detection of DNA products…… 19

Figure 5: Diagnostic Digestion (mini-Tn7 delivery vector pUC18-mini-Tn7T-Gm-*lux*) …. 20

Figure 6: Diagnostic Digestion (mini-Tn7 helper plasmid TNS2) …...……. 21

Figure 7: Constructing a bioluminescent PA strain utilizing Tn7 system…….……. 24

Figure 8: Characterization of the constructed stains growth and bioluminescence…… 25

Figure 9: Biofilm assay *in vitro*…….……. 26

Figure 10: The Model Implant and Surgical Technique……. 29

Figure 11: Systemic response to infection (Clinical outcome) ……..... 34

Figure 12: *In vivo* Imaging System (IVIS)……. 36

Figure 13: Determination of bacterial loads (Viable Colony Count)……. 37

Figure 14: Representative sections of left hip MRI…… 38

Figure 15: FE-SEM imaging of explanted implants……... 39

Figure 16: Weight-bearing and gait pattern analysis…….……. 40

Figure 17: Testing osseointegration utilizing microCT scanning……... 41

Figure 18: Complications……... 46

CHAPTER 1: INTRODUCTION

1.1 Prosthetic Joint Infection

Total joint arthroplasty (TJA) is considered one of the great medical advancements of the past half-century, by consistently allowing patients with severe pain and functional limitations to regain mobility and life quality (Convery, 1992). Over the past decade, there has been a significant increase in demand for joint replacements to manage a wide spectrum of musculoskeletal disorders such as osteoarthritis, inflammatory arthritis, and metastatic bone disease (CIHI, 2019).

According to the Canadian Joint Replacement Registry (CJRR), hip and knee replacements are the third and second most common surgeries performed in Canada, with about 130,000 done annually, 59,000 hip replacements and more than 70,000 knee replacements were performed in Canada in 2017–2018. This represents an increase of 17.4% and 17%, respectively, over the last 5 years (CIHI, 2019). Despite the significant benefits of joint replacement, prosthetic joint infection (PJI) continues to be its most common complication (Beswick et al., 2012; Kamath et al., 2015; Lenguerrand et al., 2018; Marschall et al., 2013; Matar et al., 2010; Parvizi et al., 2018; Vielgut et al., 2015) with concerning rates of morbidity and mortality (Fagotti et al., 2018).

Currently, PJI represents one of the most common causes of revision surgeries with an incidence reaching 14% in revision surgeries, and 40% in cancer patients (Armstrong et al., 2018; Jeys et al., 2005; Urish et al., 2018). PJI can be a devastating complication. It is challenging to diagnose, with severe health and socioeconomic implications and typically requires costly, resource-intensive surgical intervention, typically more than once, for successful treatment (Beswick et al., 2012; Marschall et al., 2013; Parvizi et al., 2018; Vielgut et al., 2015).

1.1.1 Epidemiology

Clinical studies and data obtained from the National Joint Registries show that PJIs occur in 0.3–1.7% and 0.5–2% of patients after total replacement of the hip and knee, respectively (Kessler et al., 2012; Laffer et al., 2006; Lenguerrand et al., 2018; Pulido et al., 2008). The incidence of PJI is anticipated to scale up proportionately with the demand for TJA, which is projected to increase substantially in the coming decade (Kurtz et al., 2018). PJI is estimated to be responsible for 15% of all revision hip and 25% of all revision knee procedures and is associated with a 5-year mortality rate higher than that of breast cancer, melanoma, Hodgkin's lymphoma, and several other common malignancies (Kurtz et al., 2018).

The incidence of PJI has remained relatively unchanged in recent years, in spite of incorporation of different strategies to reduce PJI such as skin preparation protocols, shorter operative times, use of laminar flow, body exhaust suits, decreased transfusions, perioperative antibiotics, antibiotic cement, and antimicrobial adhesive dressings (Alamanda and Springer, 2019; Jämsen et al., 2009; Kurtz et al., 2018).

1.1.2 Economic Burden

Treatment of PJI is a tremendous economic burden, as current standard therapies for PJI are very costly and have failure rates of up to 30% (Armstrong et al., 2018; Bozic and Ries, 2005; CIHI, 2019; Flemming and Wingender, 2010; Jeys et al., 2005; Kunutsor et al., 2018; Premkumar et al., 2021a; Urish et al., 2018). Data suggest about 5-fold increase in hospital expenditure compared to primary uncomplicated TJA (Akindolire et al., 2020; Bozic and Ries, 2005).

1.1.3 Gram Negative Prosthetic Joint Infection

Although the major culprits of PJI are Gram-positive (GP) organisms, Gram-negative (GN) organism-induced PJI resulted in worse clinical outcomes (Kalbian et al., 2020; Zmistowski et al.,

2011). Historically, GN-PJI was considered a rare complication, accounting for 3%–6% of all PJI (Moran et al., 2007; Del Pozo and Patel, 2009; Zimmerli et al., 2004). However, during the past 15 years, reports have uncovered higher rates of GN-PJI, ranging from 15% to 36% of all PJIs, (Benito et al., 2014, 2016; Cunningham et al., 2017; Hsieh et al., 2009; Jamei et al., 2017; Li et al., 2013; Moran et al., 2007; Peel et al., 2012; Del Pozo and Patel, 2009; Zimmerli et al., 2004), especially in immunocompromised patients (Cunningham et al., 2017). Studies have indicated that GN-PJI carries a higher risk of implant loosening even after reimplantation (Chen et al., 2019).

Pseudomonas aeruginosa (PA) is a strong predictor of poor clinical outcomes, high treatment failure rate and oftentimes require more surgeries and longer hospitalizations (Chen et al., 2019; Cunningham et al., 2017; Rodríguez-Pardo et al., 2014; Rosenthal et al., 2016; Shah et al., 2016; Zmistowski et al., 2011), especially if it develops resistance to fluoroquinolones (Cerioli et al., 2020). A clinical study has shown that PA was the most isolated pathogen (40%) of the all GN-PJI (Hsieh et al., 2009). The rates of antibiotic-resistant PA have been steadily rising with minimal progress in developing novel therapeutic alternatives (Ribera et al., 2015). The International Nosocomial Infection Control Consortium reported that PA nosocomial infections have become a worldwide healthcare issue (Rosenthal et al., 2016).

1.1.4 Treatment of PJI

In brief, three curative procedures are available options for treatment of PJI: debridement, antibiotics, and implant retention (DAIR); one-stage exchange and two-stage exchange involving variable intervals options between steps. If the appropriate intervention is selected for each patient, the overall cure rate is up to 90% (Beswick et al., 2012; Giulieri et al., 2004; Laffer et al., 2006). Patients not qualifying for any of these interventions can be treated with a palliative procedure, including implant removal without replacement or amputation. In addition, in patients with a very

high surgical risk, long-term suppressive antimicrobial therapy without surgery may be an option (Zimmerli et al., 2004). Some countries permit the use of phage therapy on compassionate grounds when all other therapies have failed or if the condition is immediately life-threatening (Gibb and Hadjiargyrou, 2021; Romero-Calle et al., 2019).

No controlled study comparing the different PJI treatment options has been conducted. Treatment recommendations are based on cohort studies, case series and expert opinion. According to data pooled from 62 relevant studies, treatment of PJI has shown an overall rate of reinfection 10.1% (8.6% and 10.2% for one-stage and two-stage revision, respectively) (Beswick et al., 2012). There is no suggestion in the published studies that one or two stage methods have different reinfection outcomes (Beswick et al., 2012). Despite the increasing clinical focus, research advances, and growing literature relating to PJI, current PJI treatment strategies remain far from optimal and no significant improvement in outcomes has been observed (Alamanda and Springer, 2019; Jämsen et al., 2009; Xu et al., 2020).

PJI treatment remains challenging, as the composite materials of the implant are susceptible to colonization by biofilm-forming bacteria (Ciofu et al., 2017; Gristina and Costerton, 1985; Tzeng et al., 2015). Biofilms protect bacteria from the immune system, antibiotic therapy and even mechanical debridement (Davies, 2003; Guzmán-Soto et al., 2021; Mah and O'Toole, 2001; Nickel et al., 1985; O'Toole et al., 2000; Olsen, 2015; Premkumar et al., 2021b; Stoodley et al., 2011). A common reason for treatment failure is inadequate debridement and removal of all diseased or devitalized tissue and bone during surgery. It is important when treating infections with a mature biofilm, to rigorously remove foreign material including implant components, cerclage wire and bone cement (Abouljoud et al., 2019; Anagnostakos and Meyer, 2019; El-

Husseiny and Haddad, 2016; Hassinger et al., 2005; Li et al., 2020; Muñoz-Mahamud et al., 2011; Urish et al., 2014).

Antibiotic treatment should be based on the type of microorganism, drug susceptibility, and the type of surgery performed. Not all antibiotics are equally active against sessile bacteria embedded in biofilm. Examples of biofilm active antibiotics are rifampicin for several GP pathogens (e.g., *Staphylococcus* species, *Cutibacterium* species) and ciprofloxacin for GN rods (Li et al., 2018, 2020). Biofilm-active therapy should be reserved for the period after implantation of the definitive implant (Li et al., 2018). For instance, infections treated with one-stage exchanges or DAIR, biofilm-active therapy should be initiated post-operatively as soon as the wounds are dry and drains removed (Li et al., 2018). Prescribing oral antibiotics with bad bone penetration and poor oral bioavailability results in insufficient local concentrations at the site of infection (e.g., beta-lactam antibiotics). Furthermore, single-drug regimens such as rifampin monotherapy should be avoided in order to minimize the risk of selecting drug-resistant micro-organisms (Zimmerli, 2014).

1.2 Biofilm

One of the most common causes of treatment failure is biofilm formation on the implant surface (Ciofu et al., 2017; Tzeng et al., 2015). Bacteria persist as a biofilm adherent to the implant surface, due to locally compromised host defense (Zimmerli and Moser, 2012). There is also a strong clinical correlation between treatment failures and the strains of microorganisms causing the infection (Fagotti et al., 2018).

1.2.1 Structure of Biofilm

Biofilms are surface-attached communities of microbial cells encased in an extracellular matrix (Barken et al., 2008; Flemming and Wingender, 2010; O'Toole et al., 2000; van Schaik et

al., 2005). Biofilm formation has been proposed as a strategy for bacteria to survive under unfavorable conditions (Davies, 2003; Guzmán-Soto et al., 2021; Mah and O'Toole, 2001; Moradali et al., 2017; Nickel et al., 1985; O'Toole et al., 2000; Olsen, 2015; Premkumar et al., 2021b; Sendi and Zimmerli, 2012; Stoodley et al., 2011). Bacterial cells undergo profound phenotypic changes during their transition from free-swimming (planktonic) cells to be a part of a complex, surface-attached community (biofilm), in response to a variety of environmental signals (O'Toole et al., 2000). For instance, bacterial cells attached to an implant surface are in a stationary phase of growth because oxygen and glucose are limited in biofilms (Sendi and Zimmerli, 2012).

Viable bacteria within biofilms are shielded and supported by the hydrated polymeric matrix known as extracellular polymeric substance (EPS). The composition and physicochemical properties of EPS are bacterial species-dependent and shaped by the environment (Flemming and Wingender, 2010). For instance, in *Staphylococcal* biofilm, following adhesion, bacterial RNA transcription changes dramatically, orienting metabolism toward anaerobic processes and production of polysaccharide intercellular adhesin (PIA), which forms the majority of the so-called slime on medical devices (Mack et al., 1996; Otto, 2008).

1.2.2 Biofilm Development *in vitro*

Many factors affect biofilm formation, including the type of microorganism, interactions with the host immune system, and the physicochemical properties of the microenvironment (Guzmán-Soto et al., 2021). The heterogenic nature of these factors causes significant complexity to study biofilms. With the intention to simulate the conditions under which biofilms develop *in vivo*, many *in vitro* biofilm models have been developed. For example, different groups have supplemented the culture media with plasma and red blood cells to develop a chronic wound biofilm model (Sun et al., 2008), cocultured epithelial cells with a multispecies biofilm to develop

a periodontal biofilm model (Millhouse et al., 2014), and assessed biofilm formation on clinically relevant arthroplasty materials to develop an *in vitro* PJI model (Premkumar et al., 2021b). While *in vitro* biofilm models are powerful tools for their reproducibility, they fail to account for the complex nature of the interactions between the host and the biofilm forming bacteria as well as the potential interaction with other bacteria (Guzmán-Soto et al., 2021). As such, the development of robust *in vivo* biofilm models is critical to validate the results from *in vitro* biofilm models.

1.2.3 *Pseudomonas aeruginosa* (PA) as a model organism to study GN-biofilm

PA has served as an important prototypic model organism for the study of GN-biofilm development *in vitro* (Hall and Mah, 2017). PA biofilm formation from individual planktonic cells is a complex developmental and highly regulated process (O'Toole and Kolter, 1998). Cells grown in biofilm are markedly different from their planktonic counterparts. For instance, PA growing on a surface has increased expression of *algC*, a gene required for the synthesis of extracellular polysaccharides (Davies and Geesey, 1995; Davies et al., 1993). The key components of EPS in PA biofilm are exopolysaccharides including Psl, Pel, and alginate, extracellular DNA (eDNA), lipids, and proteins. Extracellular type IV pili and flagella also act as structural elements within mature biofilms (Barken et al., 2008; van Schaik et al., 2005). The composition and function of EPS in the PA biofilm are highlighted in several reviews (Flemming and Wingender, 2010; Moradali et al., 2017).

It has been demonstrated that flagellar motility is important for the formation of a bacterial monolayer of abiotic surfaces by bringing the cell within close proximity of the surface to overcome repulsive forces between the bacterium and the surface to which it will eventually attach (Mills et al., 1996; O'Toole and Kolter, 1998; Simpson et al., 1995). In downstream events, type

IV pili and twitching motility play a role in stabilizing interactions with the abiotic surface and in the cell-to-cell interactions required to form a microcolony (O'Toole and Kolter, 1998).

1.2.4 Surface Attachment Deficient (*sad*) genes

It has been reported that motility is required for PA biofilm formation on biotic and abiotic surfaces and pathogenesis (Simpson et al., 1995). O'Toole and Kolter (1998) presented designated surface attachment defective (*sad*) mutants of PA (PA14), which are defective in biofilm formation. They reported the molecular characterization of two classes of mutants defective in initiation of biofilm formation: (a) mutants defective in flagellar motility and (b) mutants defective in type IV pili biogenesis and twitching motility (O'Toole and Kolter, 1998).

Mutation of the *flgK* locus results in the synthesis of an incomplete flagellum, which renders the strains non-motile (Homma et al., 1990; O'Toole and Kolter, 1998). Interestingly, a *ΔflgK* mutant is defective in initiation of biofilm formation *in vitro* on abiotic surfaces (O'Toole and Kolter, 1998). The *pilY1* gene is in a cluster of genes (including *pilV, pilW, pilX, pilY2*, and *pilE*) that is required for type IV pili biogenesis which is required for a form of surface-associated movement known as twitching motility (Alm and Mattick, 1995; Alm et al., 1996; O'Toole and Kolter, 1998; Russell and Darzins, 1994). Mutations in *pilY1* result in a non-piliated cell that did not develop microcolonies, suggesting that these structures play an important role in microcolony formation as well as stabilizing interactions with the abiotic surface (O'Toole and Kolter, 1998).

1.3 Role of Bacterial Biofilms in Implant Related Infections

Unlike pneumonia or urinary tract infection, long-term antimicrobial therapy for PJIs frequently fails (Brandt et al., 1997). Generally, PJI cannot be cured without removal of the device. However, DAIR is considered under certain conditions (Giulieri et al., 2004; Laffer et al., 2006; Zimmerli et al., 1998, 2004). Successful management of orthopaedic device-related infections

requires combined surgical and antimicrobial therapy (Sendi and Zimmerli, 2012). *In vitro* studies revealed that most antimicrobial agents have much higher minimal bactericidal concentration (MBC) during the stationary than the logarithmic phase of growth (Baldoni et al., 2009; Corvec et al., 2013; Furustrand Tafin et al., 2011, 2012; John et al., 2009; Schwank et al., 1998; Trampuz et al., 2007; Widmer et al., 1990). The high MBCs and the lack of efficacy against adherent bacteria are predictive of the failure of antibiotics in implant associated infections (Hsieh et al., 2009; Widmer et al., 1990; Zimmerli et al., 1998).

For better understanding of biofilm formation in the setting of GN-PJI and to identify the correct surgical approach for treatment, it is important to use a clinically representative *in vivo* biofilm-based GN-PJI model. In the next section, I will present an overview of different strategies to develop a clinically representative PJI animal model as reported in the literature.

1.4 Prosthetic Joint Infection Animal Models

1.4.1 Model Animal Selection

A variety of animals, including dogs, rabbits, and rodents (rats and mice), have been utilized in PJI models. Simple nonmammalian models, such as *Caenorhabditis elegans* (Diard et al., 2007), *Danio rerio* (*Zebrafish*)(Neely et al., 2002), and *Drosophila melanogaster* (de Bentzmann et al., 2012) eliminated some of the practical problems associated with the cost of small and large animals raising and housing (Ziegler et al., 2016), to be utilized in high-throughput screening studies (Letamendia et al., 2012). However, their inability to reproduce the implant-associated infection environment or present complex immune responses make them unsuitable for the study of chronic infections. Small-sized rodents require relatively low housing costs and are easy to handle. However, rodents are physiologically fragile, and surgical procedures upon them are technically demanding due to their small size. Large animal models involving dogs or sheep

are more tolerant of multiple interventions and can utilize commercially available implants. However, they can carry higher cost and additional ethical challenges (Carli et al., 2016).

The overall organization of the immune system remains consistent across mammals, but varies in cell proportions, signaling pathways, and the time after birth by which the animals become immunocompetent (Doeing et al., 2003; Felsburg, 2002; Holsapple et al., 2003). A recent review of animal models of *Staphylococcus aureus* osteomyelitis revealed dissimilarities in immune function and infection susceptibility among species (Reizner et al., 2014). The bone structure and turnover rate across mammals vary considerably. For instance, larger animals demonstrate a secondary osteonal structure (Egermann et al., 2005), with higher bone mineral density than human bone (Kimmel and Jee, 1982; Wang et al., 1998). Rabbit bone contains parallel vascular canals of osteons (Martiniaková et al., 2005), with mineral density similar to human bone (Gilsanz et al., 1988), but faster bone turnover (Castañeda et al., 2006; Newman et al., 1995). Rats and mice lack haversian systems (Nunamaker, 1998), but show similar remodeling to that observed in larger animals and humans (Holstein et al., 2009).

1.4.2 Model Implant Selection

To establish a clinically representative PJI model, it is important to utilize an implant that can reproduce the periprosthetic environment consisting of the hypovascular (immune-privileged) articular space, hypercellular intramedullary space, and the arthroplasty implant that separates the 2 environments (Carli et al., 2016) (Figure 1). Previous investigations have demonstrated bacteria respond to loading (Wijeyekoon et al., 2004) and shear forces (Liu and Tay, 2001) that affect biofilm density and strength, so it is critical to achieve stable fixation in bone following insertion and weight bearing. The immune response is similarly affected by implant stability (Fears et al., 2015).

Initial animal PJI models used loose, intramedullary implants following intramedullary bacterial inoculation (Nijhof et al., 2000; Petty et al., 1985), or inserted after coating with biofilm (Nishitani et al., 2015). These models were limited in translational appeal because of inaccurately recreating the periprosthetic environment, since their implants were loose and do not bear weight. Transcortical screws into the distal part of the femur (Craig et al., 2005) or stemmed silicone-elastomer implant in the rabbit tibia (Belmatoug et al., 1996), have been utilized followed by intra-articular bacterial inoculation. Unfortunately, the unrepresentative nature of the material used decreases enthusiasm for these approaches. A novel PJI mouse model that utilized a 3D-printed medical grade titanium implant that bears load in a manner similar to that of a human tibial component has been proposed as a clinically representative PJI model (Carli et al., 2016, 2017; Yang et al., 2015). However, this model tested only GP-PJI (*S. aureus*). Furthermore, the osseointegration for this model was not quantitatively assessed.

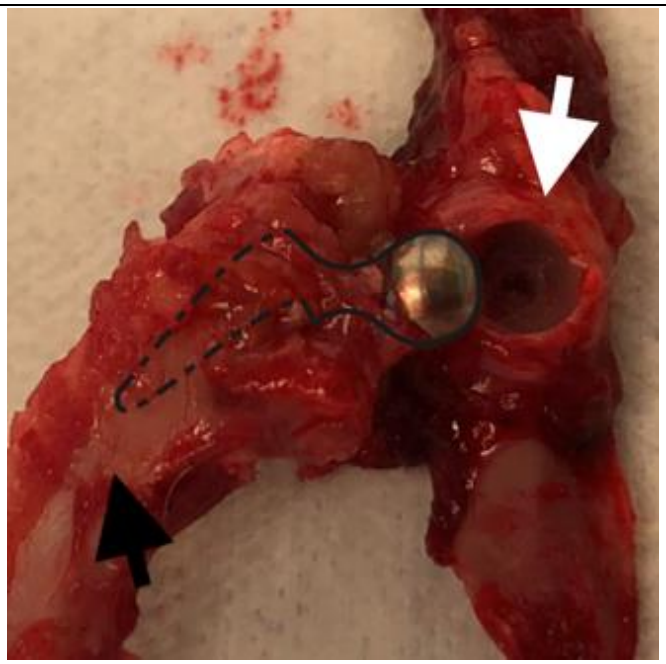

Figure 1: Hip Hemiarthroplasty model implant reproduces the periprosthetic environment consisting of the hypovascular (immune-privileged) articular space (white arrow: hip joint), hypercellular intramedullary space (black arrow: femoral medulla), and the arthroplasty implant that separates the 2 environments (Solid line: implant head and neck; Dashed line: implant stem inside the femoral canal)

1.4.3 Model Organism (Pathogen) Selection

To select the pathogens inducing PJI (model organisms), common clinical pathogens should be utilized. It is important to be aware of the similarities and differences in virulence and biofilm formation of the proposed model organisms. Although the major culprits of PJI are GP organisms, GN organisms resulted in worse clinical outcomes PJI (Fagotti et al., 2018; Kalbian et al., 2020). Most of the PJI animal models have focused on GP infection, especially *S. aureus* and *S. epidermidis* (Carli et al., 2017; Lovati et al., 2017).

Since GN bacteria differ from GP bacteria in many ways, including their mechanisms of virulence (Cohen, 2001; Ramachandran, 2014), biofilm formation (López et al., 2010; O'Toole et al., 2000), and host immune responses (Abe et al., 2010; Skovbjerg et al., 2010), there is a need to design clinically representative animal models for GN-PJI to better understand its pathogenesis and to test the safety and efficacy of novel therapies. Thompson et al (Thompson et al., 2018), recently developed a GN-PJI *in vivo* model using a Kirschner-wire which was surgically implanted into the femoral canal of mice, with its end protruding into the knee joint. GN-PJI was induced by a more virulent PA infection, and a less virulent *E. coli* infection. However, this model still lacks the accurate clinical depiction of the periprosthetic joint environment since it does not articulate within a weightbearing joint nor does it allow for implant osseointegration (Thompson et al., 2018). Another limitation of this model as it employed *E. coli* (Xen14) as low biofilm-producing strain but it was indicated to induce biofilms by *in vitro* biofilm assay (Nowatzki et al., 2012).

The method of bacterial inoculation must be carefully considered. Previous PJI models either have directly administered bacteria into the operative site (Belmatoug et al., 1996; Bernthal et al., 2010; Craig et al., 2005; Niska et al., 2012; Pribaz et al., 2012) or have pre-grown biofilm on an implant surface prior to implantation (Li et al., 2008; Nishitani et al., 2015).

1.5 Outlook and Clinical Significance

GN-PJI portends a higher risk of aseptic loosening after reimplantation, mainly because of the lipopolysaccharide (LPS)-mediated effects on osteoclast differentiation (Chen et al., 2019). Therefore, there is a need to design clinically representative animal models for GN-PJI to better understand its pathogenesis and to test the safety and the efficacy of novel therapies.

The animal model described in our current study uses a unique ball-in-socket 3D-printed, medical-grade titanium (Ti-6Al-4V) implants that replace native femoral heads of Sprague-Dawley rats and articulate congruently with their native acetabula (Paish et al., 2020). The stem of the implant sits anatomically within the femoral canal with a roughened surface to enhance stability and bone ingrowth (Figure 1). This model can bear weight, translating important clinical features of prosthetic joint in humans more accurately.

The main aim of this study is to establish a clinically representative GN-PJI model that can reliably recapitulate biofilm formation on titanium implant surface *in vivo*. A secondary aim was to correlate biofilm formation with implant loosening. In order to achieve these aims, two PA strains were utilized: 1) A highly virulent clinical isolate from a human burn patient (Hao et al., 2015; Mikkelsen et al., 2011), that has been used extensively as a model organism for biofilm formation on abiotic and biotic surfaces (PA14) (Govan and Deretic, 1996; O'Toole and Kolter, 1998). 2) A biofilm-defective strain (*ΔflgK*) (Homma et al., 1990; O'Toole and Kolter, 1998). It has been demonstrated that flagellar motility is required for PA to form a biofilm (O'Toole and Kolter, 1998; Simpson et al., 1995). Mutation of the *flgK* locus results in the synthesis of an incomplete flagellum, which renders non-motile strain (*ΔflgK*) and defective in biofilm formation *in vitro* (Homma et al., 1990; O'Toole and Kolter, 1998). I hypothesized that the biofilm formation on the implant surface would negatively affect its ability to osseointegrate.

CHAPTER 2: METHODS

2.1 Experimental Design

The GN-PJI model was developed based on 3D-printed, medical-grade, titanium (Ti-6Al-4V), cementless hip hemiarthroplasty implants (Paish et al., 2020), to partially replace the left femoral heads of Sprague-Dawley rats. Figure 2 summarizes the timeline and experimental design.

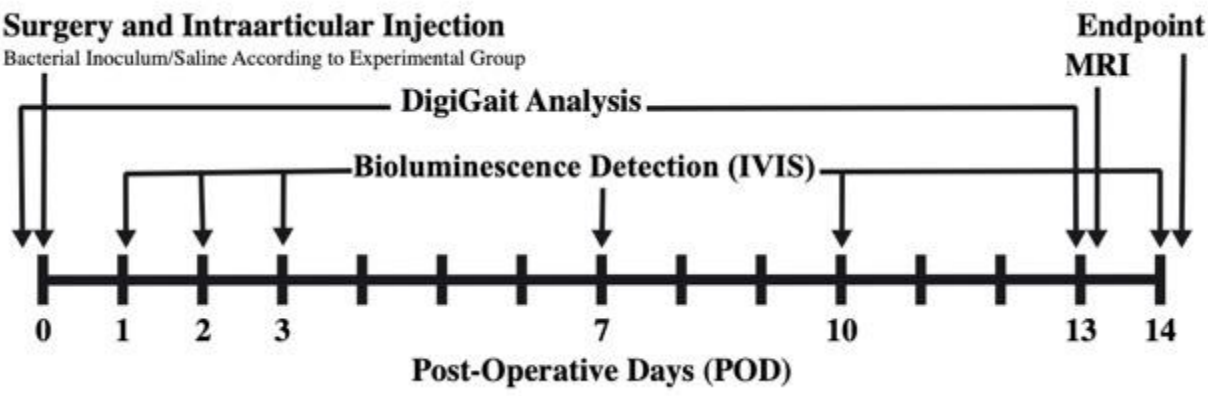

Figure 2: Experiment Timeline
IVIS (*in vivo* Imaging System), MRI (Magnetic Resonance Imaging), POD (Post-Operative Days)

2.2 Model Organism

To induce GN-PJI, PA was selected as a model organism (pathogen). PA has served as an important prototypic model organism for the study of GN-biofilm development *in vitro* (Hall and Mah, 2017; O'Toole and Kolter, 1998; O'Toole et al., 2000). PA strain (PA14) was selected to induce PJI to establish an *in vivo* biofilm-based GN-PJI model. PA14 is a highly virulent clinical isolate from a human burn patient (Hao et al., 2015; Mikkelsen et al., 2011), that has been used extensively as a model organism to test biofilm formation on abiotic and biotic surfaces (Govan and Deretic, 1996; O'Toole and Kolter, 1998). To be able to highlight the effect of biofilm formation in the setting of GN-PJI, it was important to identify a PA14 mutant that is defective in biofilm formation to serve as a negative control for the *in vivo* GN-PJI model.

2.2.1 Determination of a Negative Control for *in vivo* Model

In order to select a strain defective in biofilm formation that could serve as a negative control for the *in vivo* model, I tested 3 designated surface attachment defective (*sad*) mutants PA14 strains obtained from George A. O'Toole's lab; a pili-defective mutant: *ΔpilY1* (O'Toole and Kolter, 1998); and flagella-defective mutants: *ΔflgK* (O'Toole and Kolter, 1998) and *ΔfliC* (Wolfgang et al., 2004). Biofilm formation *in vitro* was tested first on plastic polyvinylchloride (PVC) utilizing a simple, highly reproducible microtiter biofilm assay (Christensen et al., 1985; Merritt et al., 2005; O'Toole and Kolter, 1998). Biofilms formation on the titanium implants were tested using Air Liquid Interface (ALI) assay principle (Caiazza and O'Toole, 2004) and direct enumeration of viable bacteria in biofilm that were attached to the implant surface.

Microtiter Biofilm Assay: The 3 designated PA *sad* mutants were screened in microtiter dishes made of polyvinylchloride (PVC) to test for their ability to form a biofilm on an abiotic surface, using a technique described previously (O'Toole and Kolter, 1998). Each strain of interest was inoculated at 37°C in 5 ml Luria-Bertani (LB) broth on a roller drum at 90 rpm for 16 h and grown to stationary phase. Cultures were diluted 1:100 in minimal medium, consisted of M63 salts supplemented with L-arginine (0.4%) and MgSO4 (1 mM). Diluted cultures for each tested strain were pipetted into four wells (100 µl each) in a fresh microtiter plate. Lids were used to cover the plates and incubated at 37°C. After a 24 h incubation at 37°C, planktonic bacterial cells were removed by shaking the dish out over the waste tray, then washed by submerging the plate in water tray and then vigorously shaking out the liquid over the waste tray. The biofilm was detected by staining with crystal violet (CV), a purple dye that stains the bacterial cells but does not stain the PVC plastic. After addition of 125 µl of 0.1% CV solution to each well and incubation at room temperature for 10 min, excess CV and unattached cells were removed by vigorous and repeated

washing of the microtiter plates with water, then the plates are allowed to dry. The flagellar-defective mutants were less adherent to PVC plastic surface versus the pili-defective mutant (Figure 3A).

Biofilm Assay on Titanium: Biofilms formation on the titanium implants was tested using Air Liquid Interface (ALI) assay principle (Caiazza and O'Toole, 2004) and direct enumeration of viable bacteria in biofilm that were attached to the implant surface. Each strain of interest was inoculated at 37°C in 5 ml Luria-Bertani (LB) broth on a roller drum at 90 rpm for 16 h. Cultures were diluted 1:100 in minimal medium, consisted of M63 salts supplemented with L-arginine (0.4%) and MgSO4 (1 mM). A sterile, flat-bottom, 12-well plate is adjusted to sit at a 30°-50° angle from horizontal by positioning one end of the plate to be rested on a microcentrifuge tube rack and stabilized with tape to prevent slipping. The 3D-printed titanium implant was consistently positioned inside each well so that one side is rested on the bottom of the well and the lateral border rested against the wall of the well. An aliquot (350 µl) of each diluted culture was carefully pipetted into each well so that the meniscus of the medium is at the center of the implant. Lids were used to cover the plates and incubated at 37°C for 24 h (Figure 3B).

Each implant was removed from its well and rinsed off nonadherent cells by dipping in sterile medium 3 times. Each implant was inserted with 1mm sterile media in an Eppendorf© Microcentrifuge tube. Samples were sonicated individually in a water bath for 15 min at 40 kHz (Branson™ 3510) to dislodge attached bacteria. The resulting suspensions from the sonicated implants and the homogenized periprosthetic tissue were serially diluted, then 10 µl plated on LB-agar 1.5% agar, and incubated overnight at 37°C (drop-plate method for bacterial enumeration (Herigstad et al., 2001)) (Figure 3C).

Viable colony count of the sonicated implants resulting suspension showed a statistically significant reduction in the bacterial loads associated with implants from the *ΔflgK* (n=4) versus the PA14 (n=4); p<0.001, with less significant reduction for the *ΔfliC* (n=4); p<0.01 and *ΔpilY1* (n=4); p<0.05 (Figure 1C).

Interestingly, repression of *fliC* (encodes flagellin) occurs *in vivo* as an adaptive response that allows *P. aeruginosa* to avoid detection by host defense mechanisms and phagocytosis during the chronic phase of cystic fibrosis lung infections (Wolfgang et al., 2004). For these reasons, *ΔflgK* was selected as the strain that is defective in biofilm formation that might serve as a negative control for the *in vivo* model.

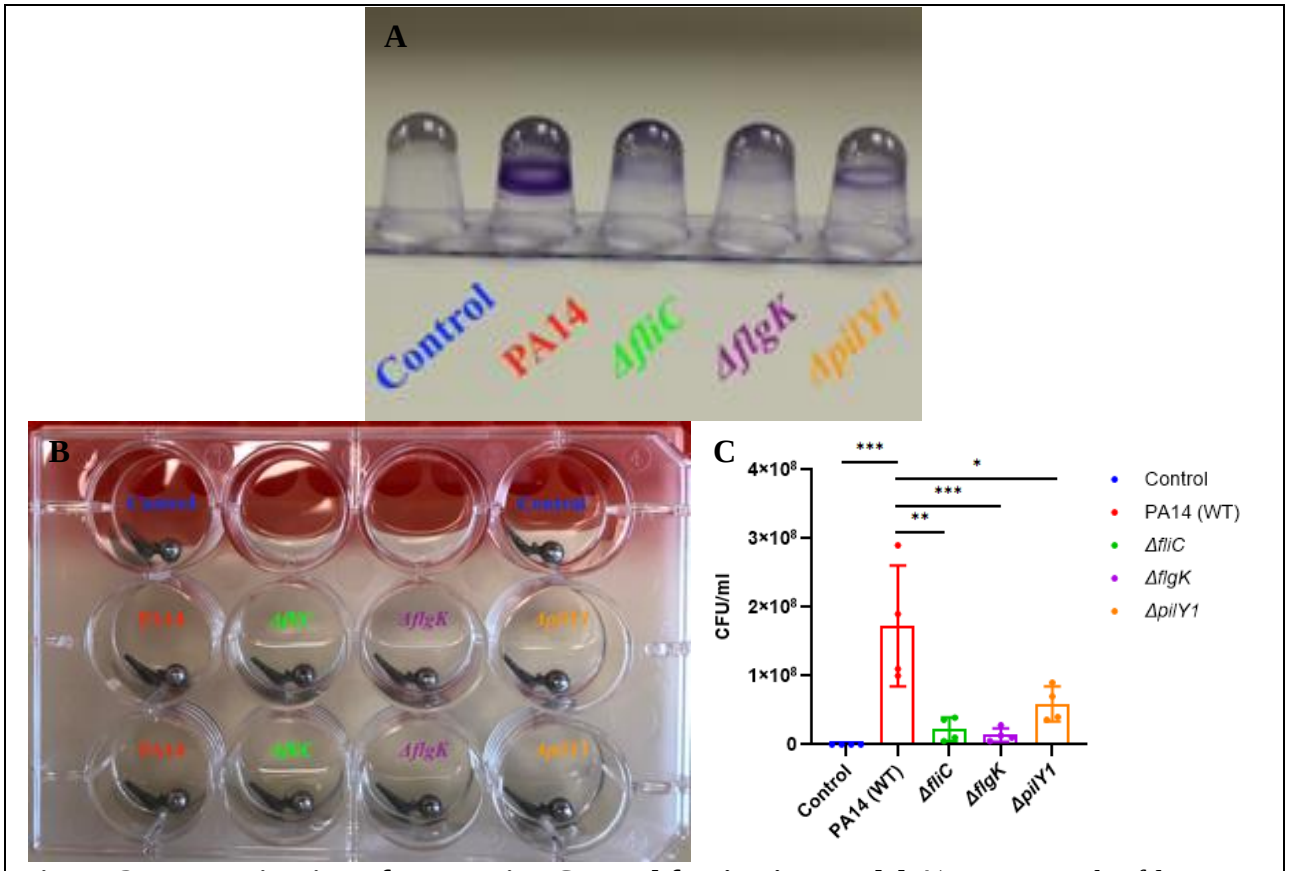

Figure 3: Determination of a Negative Control for *in vivo* Model A) microtiter biofilm assay B) 12-well plate with titanium implants setup for Air-Liquid-Interface Biofilm Assay C) Air-Liquid-Interface Biofilm Assay on titanium implant surface and direct bacterial enumeration of sonicated implants resulting suspension (mean viable-colony-counts CFU/mL ± standard deviation n=4) (* p-value <0.05; ** p-value <0.01; *** p-value <0.001).

2.2.2 Construction of Bioluminescent PA Strains

For non-invasive monitoring of PJI in real-time and quantitative assessment of biofilm formation *in vivo*, bioluminescent PA strains (PA14-*lux* and *ΔflgK*-*lux*) were constructed by employing the mini-Tn7 system (Choi and Schweizer, 2006; Choi et al., 2005) to integrate the *lux* operon into the bacterial chromosome. Since PA14-*lux* was constructed by a former student in the Mah lab, Clayton Hall, I constructed a bioluminescent version of a PA14 mutant (*ΔflgK*-*lux*) that is defective in biofilm formation *in vitro* utilizing the same system.

2.2.3 Mini-Tn7 System

Briefly, a mini-Tn7 suicide delivery vector (pUC18-mini-Tn7T-Gm-*lux*), which carries the *lux* operon and a helper plasmid (pTNS2) which carries the genes encoding components of the *TnsABCD* site-specific transposition pathway) were transferred into the recipient cell (*ΔflgK*) by electroporation. Transformants contain the transposon inserted into the chromosome with a single *att*-Tn7 site 25 nucleotides downstream of the respective *glmS* genes. The primer pairs $P_{glmS\text{-}down}$-P_{Tn7R} were used to verify the transposition event by colony PCR to detect insertions at *att*-Tn7. Electrophoresis on a 1% agarose gel was used to analyze PCR reactions.

2.2.4 Plasmid DNA Purification

Purification of mini-Tn7 suicide delivery vector pUC18-mini-Tn7T-Gm-*lux* (plasmid carrier for *lux* gene) from carrier strain *E. coli* HPSI pUC18-mini-Tn7T-Gm-*lux*.

Purification of mini-Tn7 helper plasmid pTNS2 (encodes transposase to integrate the *lux* gene into the bacterial chromosome) from carrier strain *E. coli* DH5α TNS2 (Table 1).

Table1: Plasmids Utilized for mini-Tn7

Mini-Tn7 plasmids	Length (bp)	Plasmid	Carrier Strain	TFM#
suicide delivery vector	11299	pUC18-mini-Tn7T-Gm-*lux*	*E. coli* HPSI	93
helper plasmid	9619	pTNS2	*E. coli* DH5α	86

For the plasmid purification, EZ-10 Spin column Kit (Bio Basic©) mini-prep was utilized. The plasmid DNA is selectively adsorbed in silica gel-based EZ-10 Spin column Kit (Bio Basic INC©) mini-prep and other impurities such as proteins, salts, nucleotides, oligos were washed away. The plasmid DNA was then eluted off the column to be used for downstream application.

The purified DNA product was detected by running agarose gel electrophoresis (Figure 4) and the concentration was measured using NanoDrop™ 2000/2000c Spectrophotometers Thermo Scientific™.

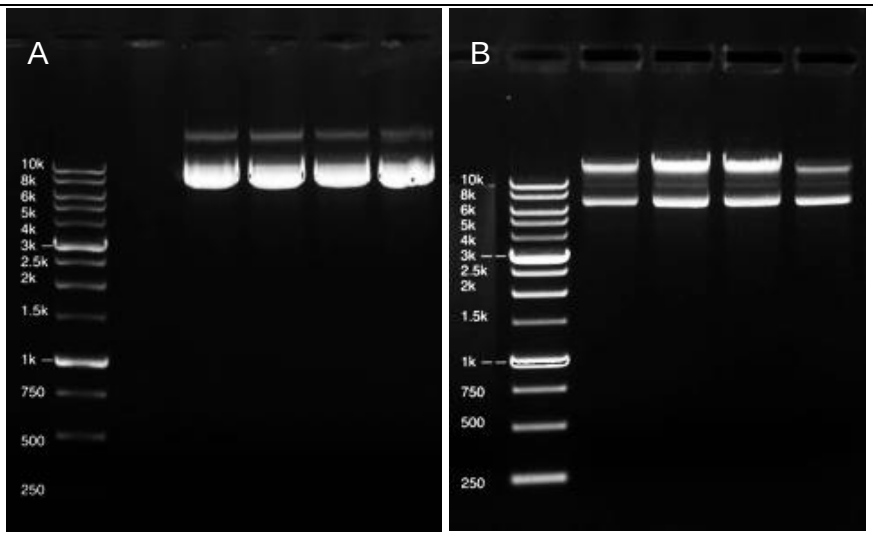

Figure 4: Detection of DNA products by running agarose gel electrophoresis A) lane 1 contains DM3100 Excel-Band™ 1 KB (0.25-10 kb) DNA Ladder (SMOBIO©), lane 2 is empty and lanes 3-6 are quadruplicates of mini-Tn7 suicide delivery vector pUC18-mini-Tn7T-Gm-*lux* and B) lane 1 contains DM3100 Excel-Band™ 1KB (0.25-10kb) DNA Ladder (SMOBIO©), lane 2-5 are quadruplicates of mini-Tn7 helper plasmid pTNS2.

2.2.5 Diagnostic Restriction Enzyme Digestion

Single digest was utilized to confirm the isolated plasmid total size. The plasmid identity was confirmed by Plasmid Fingerprinting; as the plasmid was cut into 3-5 pieces such that all fragments are small enough to be accurately sized on a gel, such that they are different enough in size to be easily resolved from each other. Using NEB-cutter© software v2.0 (Vincze et al., 2003),

for pUC18-mini-Tn7T-Gm-*lux*, enzymes KnpI (single cut, Linear DNA), EcoRI (2 cuts, 2 fragments) and double KpnI and EcoRI (3 cuts, 3 fragments), were identified (Table 2, Figure 5).

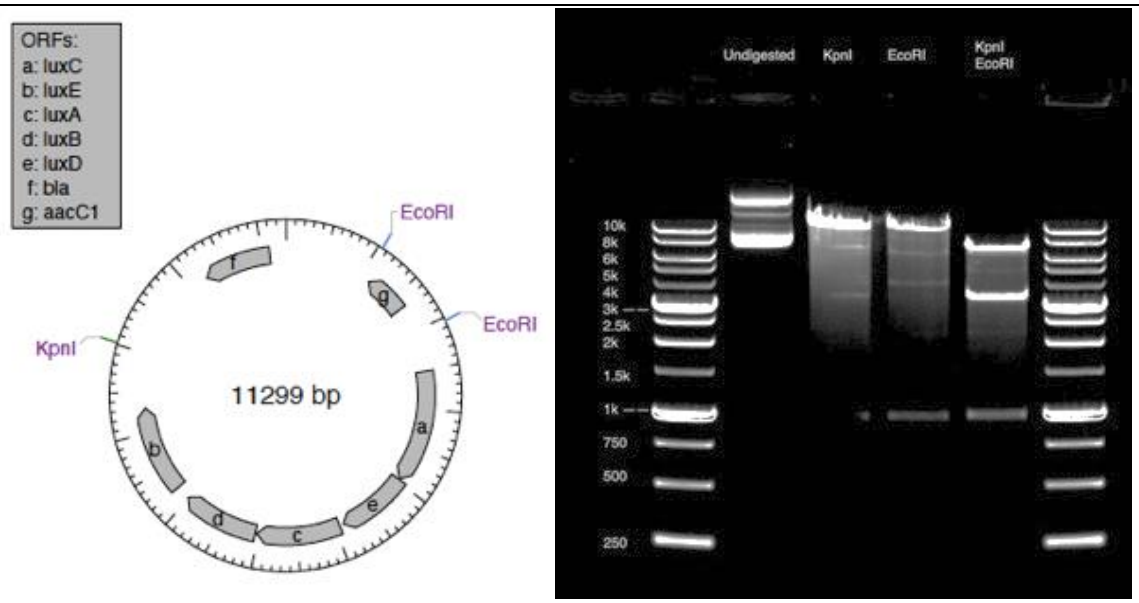

Figure 5: Diagnostic Digestion for mini-Tn7 delivery vector pUC18-mini-Tn7T-Gm-*lux* A) Image created by NEB-cutter© software (v2.0)(Vincze et al., 2003) displaying the sequence digested with: EcoRI, KpnI. B) Agarose gel electrophoresis. Lane 1 contains DM3100 Excel-Band™ 1KB (0.25-10 kb) DNA Ladder (SMOBIO©). Lane 2 contains undigested DNA product. Lane 3 contains KnpI enzyme digestion (single cut, Linear DNA). Lane 4 contains EcoRI enzyme digestion (2 cuts, 2 fragments). Lane 5 contains KpnI and EcoRI double enzyme digestion (3 cuts, 3 fragments).

Table 2: Diagnostic Digestion for mini-Tn7 delivery vector pUC18-mini-Tn7T-Gm-*lux*

#	Ends	Coordinates	Length (bp)
Single cut (Linear DNA)			
1	KpnI-KpnI	9024-9023	11299
2 cuts, 2 fragments			
1	EcoRI-EcoRI	2037-1048	10311
2	EcoRI-EcoRI	1049-2036	988
3 cuts, 3 fragments			
1	EcoRI-KpnI	2037-9023	6987
2	KpnI-EcoRI	9024-1048	3324
3	EcoRI-EcoRI	1049-2036	988

For helper plasmid TNS2, EcoRI (single cut, Linear DNA), BamHI (4 cuts, 4 fragments), HindIII (5 cuts, 5 fragments) and XbaI (4 cuts, 4 fragments), were identified (Table 3, Figure 6).

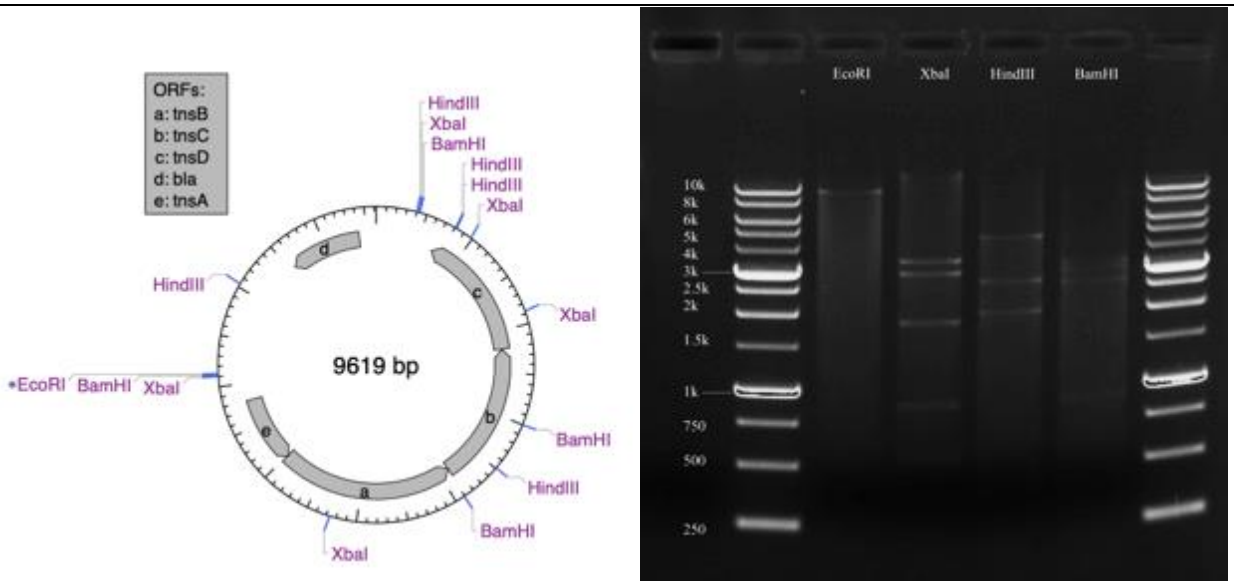

Figure 6: Diagnostic Digestion for mini-Tn7 helper plasmid TNS2 A) Image created by NEB-cutter© software (v2.0)(Vincze et al., 2003) displaying the sequence digested with: EcoRI, BamHI, HindIII and XbaI. B) Agarose gel electrophoresis. Lane 1 contains DM3100 Excel-Band™ 1KB (0.25-10kb) DNA Ladder (SMOBIO©). Lane 2 contains EcoRI enzyme digestion (single cut, Linear DNA). Lane 3 contains XbaI enzyme digestion (5 cuts, 5 fragments). Lane 4 contains HindIII enzyme digestion (5 cuts, 5 fragments). Lane 5 contains BamHI enzyme digestion (4 cuts, 4 fragments).

Table 3: Diagnostic Digestion for mini-Tn7 helper plasmid TNS2

#	Ends	Coordinates	Length (bp)
Single cut, Linear DNA			
1	EcoRI-EcoRI	7131-7130	9619
5 cuts, 5 fragments			
1	XbaI-XbaI	1876-5266	3391
2	XbaI-XbaI	7104-423	2939
3	XbaI-XbaI	5267-7103	1837
4	XbaI-XbaI	986-1875	890
5	XbaI-XbaI	424-985	562
5 cuts, 5 fragments			
1	HindIII-HindIII	3493-8037	4545
2	HindIII-HindIII	819-3492	2674
3	HindIII-HindIII	8038-399	1981
4	HindIII-HindIII	400-807	408
5	HindIII-HindIII	808-818	11
4 cuts, 4 fragments			
1	BamHI-BamHI	3906-7109	3204
2	BamHI-BamHI	7110-429	2939
3	BamHI-BamHI	430-3003	2574
4	BamHI-BamHI	3004-3905	902

2.2.6 Constructing a bioluminescent PA strain utilizing Tn7 system

The mini-Tn7 suicide delivery vector (pUC18-mini-Tn7T-Gm-*lux*) which carries the *lux* operon and Gentamicin resistance (GmR) selection marker and the helper plasmid (pTNS2), which carries the genes encoding components of the TnsABCD site-specific transposition pathway, were transferred into the recipient cell by electroporation. Transformants contain the transposon inserted into the chromosome with a single *att*Tn7 site 25 nucleotides downstream of the respective *glmS* genes.

Preparation of Electrocompetent Cells: PA strain was inoculated at 37°C in 6 ml LB broth on a roller drum at 90 rpm for 16 h. The whole culture was distributed evenly into four sterile microcentrifuge tubes and centrifuged at 16,000 g and room temperature for 2 min. The supernatant was removed. Each cell pellet was suspended in 1 ml of 300 mM sucrose (at room temperature), then centrifuged at 16,000 g and room temperature for 2 min, and this was repeated twice. The four cell pellets were suspended in a combined volume of 200 µl of 300 mM sucrose.

DNA transformation 100 µl of electrocompetent cells were transferred to a 2 mm gap-width electroporation cuvette. Using a 1–100 µl gel-loading tip, 50 ng of mini-Tn7 element DNA (pUC18-mini-Tn7T-Gm-*lux*) and 50 ng of pTNS2 were added and mixed by gentle stirring with the gel-loading pipette tip to avoid air bubbles. (The DNA was electroporated into the cells using the following settings: 25 µF, 200 Ω, 2.5 kV (the time constant should be <5 ms). 1 ml of LB medium was immediately added (to facilitate immediate recovery from the electroshock) and incubated with shaking (225 rpm) for 1 h at 37℃. 100µl of the mixture was plated on LB 1.5% agar with 20 µg/ml Gentamicin plate. Plates were incubated at 37℃ overnight or until colonies appeared. Bioluminescence activity of the colonies was assessed using the IVIS (Figure 7A).

Confirmation of proper insertions at attTn7 by colony PCR The primer pairs $P_{glmS\text{-}down}$-P_{Tn7R} were used to verify transposition event by colony PCR to detect single site insertion at *att*Tn7 (Table 4).

Table 4: List of Primers for Pair Primer Colony PCR

Primer	Sequence	Concentration
P_{Tn7R}	5`-CACAGCATAACTGGACTGATTTC-3`	30pmol/µl
$P_{glmS\text{-}down}$	5`-GCACATCGGCGACGTGCTCTC-3`	30pmol/µl

Single, large colony from GmR transformant was picked and transferred into a sterile microcentrifuge tube containing 30 µl of sterile H2O and boiled for 5min. Cell debris was pelleted by centrifuging for 2 min at 16,000 g and room temperature in a microcentrifuge. 25 µl of supernatant was transferred to a fresh microcentrifuge tube and placed on ice. The components listed in Table 5 were combined and run in a PCR reaction using the conditions listed in Table 6.

Table 5: Ingredients for PCR

Component	Amount (µl)
ddH_2O	35.0
10 mM dNTPs	2.0
10x *Taq* buffer	5.0
50 mM $MgSO_4$	4.0
Supernatant DNA	2.0
30pmol/µl P_{Tn7R}	0.25
30pmol/µl $P_{glmS\text{-}down}$	0.25
5 U/ml *Taq* polymerase	1.5
Total	50.0

Table 6: PCR conditions

Cycle number	Denaturation	Annealing	Extension
1	95℃, 5min	None	None
2-31	95℃, 45 s	59℃, 30 s	72℃, 20 s
32			72℃, 10 min

20 µl aliquots of the 50-ml PCR reactions were analyzed by gel electrophoresis on a 1% agarose gel in Tris-acetate-EDTA (TAE) buffer (run at a constant 100–120 V for 30 min). Using

the P_{Tn7R}-$P_{glmS\text{-}down}$ primer pair and the PCR cycle conditions indicated, a single PCR fragment of 272 bp was observed with DNA from GmR transformants. This fragment will be absent when using a DNA template derived from PA14 and *ΔflgK* (negative control) (Figure 7B).

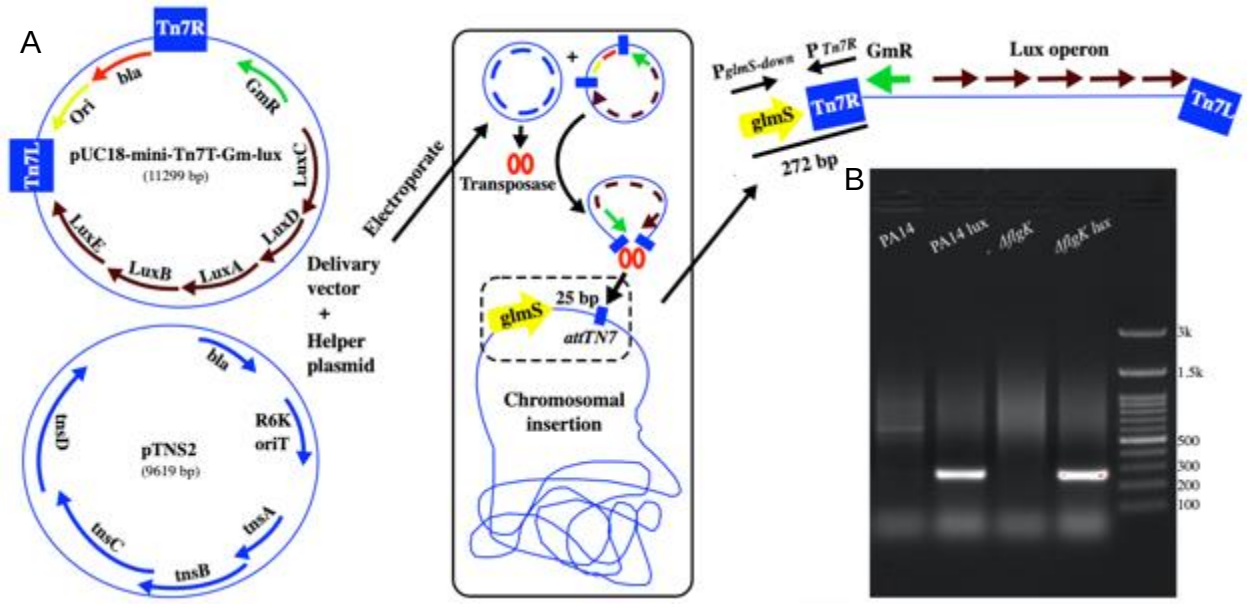

Figure 7: Constructing a bioluminescent PA strain utilizing Tn7 system A) The mini-Tn7 suicide delivery vector (pUC18-mini-Tn7T-Gm-*lux*) and the helper plasmid (pTNS2), transferred into the recipient cell by electroporation. Transformants contain the transposon inserted into the chromosome with a single *att*Tn7 site 25 nucleotides downstream of the respective *glmS* genes. The primer pairs $P_{glmS\text{-}down}$-P_{Tn7R} shown by convergent arrows are used to verify transposition event by colony PCR to detect insertions at *att*Tn7. B) Electrophoresis on a 1% agarose gel was used to analyze 20-ml aliquots of the 50 ml PCR reactions. Lane 1 contains PCR products obtained from wild-type PA14 (negative control); lane 2 contains PCR products from PA14 *lux* (positive control); lane 3 contains PCR products from *ΔflgK* (negative control); lane 4 contains PCR products from *ΔflgK lux*; Lane 5 contains DM2300 Excel-Band™ 100 bp+3K DNA Ladder (SMOBIO). bla (beta lactamase), GmR (gentamicin resistance).

2.2.7 Characterization of the Constructed Strains

To confirm that the constructed strains (PA14 *lux* and *ΔflgK lux*) had no growth defects, optical density (absorbance endpoint; λ=600 nm) measured every 30 min for 18 h at 37°C and shaking frequency=355 cpm. For each strain, 4 replicate measurements were performed in separate wells of the same plate in the microplate reader (Synergy™ H1, BioTech™) as well as the

corresponding bioluminescence measurements in relative light units/Sec (RLU/Sec) (Figure 8A-B). Bioluminescent activity of the streak out constructed strains on LB agar plates was detected using the *in vivo* imaging system IVIS (PerkinElmer™) (Figure 8C).

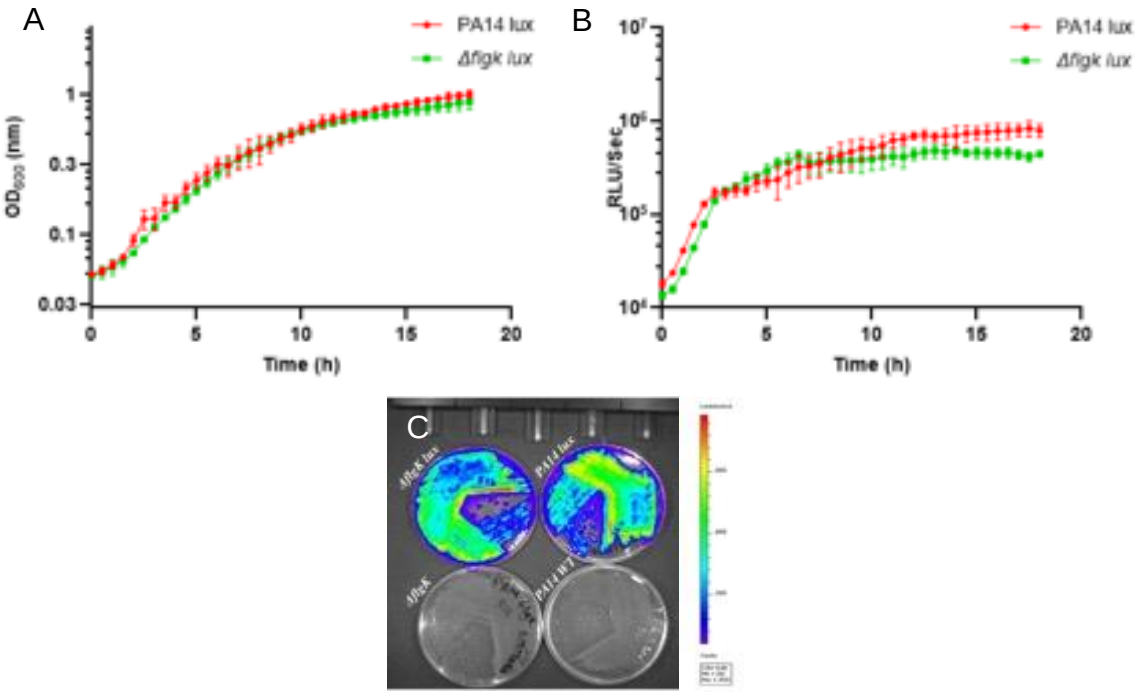

Figure 8: Characterization of the constructed stains growth and bioluminescence A) OD curve for PA14-*lux* and *ΔflgK-lux* measured at $\lambda = 600$ nm every 30 min for 18 h. The depicted curve is the mean value of 4 replicate measurements performed in separate wells of the same plate in the microplate reader (Synergy H1, BioTech™). Error bars are the standard deviation of the mean. Where the error bars are not visible, they are smaller than the data symbols. The OD saturates when N is large enough to deplete the nutrient sources in the media. B) Corresponding bioluminescence measurements in relative light units/Sec (RLU/Sec). C) Detection of bioluminescent activity using the *in vivo* imaging system IVIS (PerkinElmer™). *ΔflgK-lux* and PA14-*lux* (on top left and right, respectively) versus *ΔflgK and* PA14 WT (on bottom left and right, respectively) were plated on LB-agar plates.

Biofilm formation by the constructed strains was tested first on plastic (PVC) utilizing a simple, highly reproducible *in vitro* microtiter biofilm assay (Christensen et al., 1985; Merritt et al., 2005; O'Toole and Kolter, 1998) (Figure 9A-B), then on titanium implants using Air Liquid Interface (ALI) assay principle (Merritt et al., 2005)(Figure 9C). Field emission scanning electron microscopy (FE-SEM) was utilized to visually confirm the defective biofilm formation of the

constructed strain *ΔflgK lux* versus the reference strain PA14 *lux* (Figure 9D-F), see section **2.4.6** (page 33).

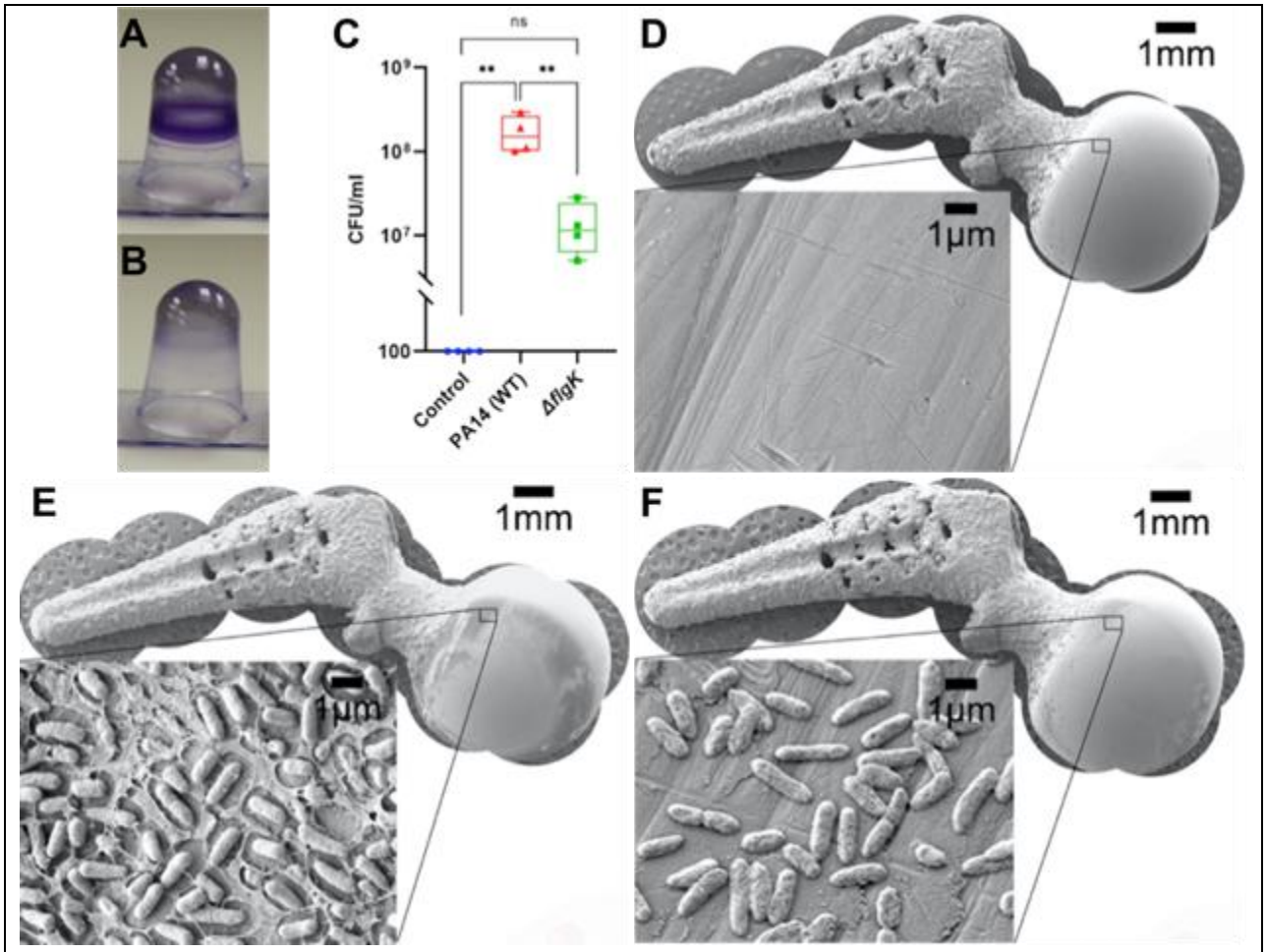

Figure 9: Biofilm assay *in vitro*
Microtiter Biofilm Assay on plastic for A) PA14-*lux* and B) *ΔflgK-lux*. C) **Air-Liquid-Interface Biofilm Assay** on titanium implant surface and direct bacterial enumeration of sonicated implants resulting suspension (mean viable-colony-counts CFU/mL ± standard deviation n=4) (* p-value <0.05; ** p-value <0.01; *** p-value <0.001). **Scanning electron microscope** (25x magnification, scale bar=1mm) of D) negative control titanium implant (sterile media) versus, E) PA14-*lux* biofilm formation with bacterial cells embedded in extracellular matrix, and F) *ΔflgK-lux* individual cells attached to the implant surface (inset image 10 k x magnification, scale bar=1 µm).

2.3 Model System

A total of 44 skeletally mature (approximately 12-week-old) Sprague-Dawley male rats were utilized. Infection was induced by intraarticular injection of bioluminescent PA strains

(PA14-*lux* and *ΔflgK-lux*) to facilitate monitoring of infection in real-time, utilizing the *in vivo* imaging system (IVIS). Weight ranged from 494-674 gm, with means 559.5 gm (509-649 gm), 554.4gm (494-661 gm) and 550.2 (511-674 gm) for non-infected surgical control, PA14-*lux* and *ΔflgK-lux* PJI groups respectively. All animal experiments followed protocol (OHRIe-3369) approved by the Animal Research Ethics Committee, University of Ottawa. Rats were housed at the University of Ottawa, Canada, animal care facility. Free access to water, a standard amount of rodent food (protein 226 g/kg, fat 50 g/kg, and 3,030 kcal/kg) were provided. The environmental temperature was adjusted between 20ºC to 24ºC with humidity between 40% to 70%, and on 12 h light-dark cycle.

2.3.1 Model Implant

Cementless hip hemiarthroplasty medical-grade titanium implants (Ti-6Al-4V) were 3D-printed by the research group at the Bone & Joint Institute, University of Western Ontario, Canada, using a selective laser melting SLM-3D-printer (AM-400; Renishaw plc, New Mills Wotton-under-Edge, UK)(Paish et al., 2020). A monobloc design with an approximated sphere femoral head and a reduced neck diameter was used to minimize the femoral acetabular impingement. The implant was designed with a collar to improve primary stability and 0.5 mm hexagonal porosity to improve bone ingrowth (Figure 10A). Prior to surgery, implants were washed in an ultrasonic bath of detergent, rinsed with water, dried, and then sterilized via autoclave.

2.3.2 Surgical Procedure

A previously described posterior approach for cemented hip hemiarthroplasty model (Hadden et al., 2021) was utilized. Pre-anesthesia administration of 5 ml fluids (0.9% sodium chloride) were given subcutaneously. To lower the dose of anesthetics needed and for postoperative analgesia, slow-release buprenorphine (0.05 mg/kg) used in conjunction with

anesthesia. To improve the safety, and to minimize the risk of drug induced respiratory depression, the analgesia protocol was modified by administrating only half dose of slow-release buprenorphine preoperatively, and the remaining half during the recovery. General anesthesia was induced with isoflurane delivered at 3.5%–4.5% gas in oxygen to induction chamber (Godbey, 2016). Once anesthesia was induced, the animal was quickly removed from the induction chamber and attached to a nonrebreathing anesthetic circuit with a tight-fitting nose cone which isoflurane delivery is then maintained with a concentration of 1.5%–3% (Godbey, 2016). To minimize corneal dryness and damage, nonmedicated ophthalmic ointments was placed in the eyes immediately after anesthetic induction (Godbey, 2016).

Lateral decubitus position, left up, was secured followed by shaving, sterile preparation with chlorhexidine, and sterile draping. Skin incision (~2 cm) was made in line with the posterior aspect of the left femur centered on the hip joint. The gluteus maximus muscle was split in line with the skin incision, retracted, and the sciatic nerve was identified and protected. The hip was then internally rotated to stretch, expose, and incise the piriformis tendon to expose the underlying capsule before capsulotomy. The ligamentum teres was released, and the femoral head was dislocated by hip adduction and internal rotation.

A fine-tipped dental burr was then used for femoral head resection. For the cementless model, a conservative neck cut was performed to retain the calcar for implant primary stability (Figure 10B-C). The femur was prepared using a series of dental files to hand ream the medullary cavity and press fit the stem within the femoral canal, using an impactor tool and a small hammer. Femoral component version simulating the native rat hip alignment was assessed utilizing the thigh-foot angle (Figure 10D), then forceps were used to grasp the implant, to ensure its stability before the joint was relocated and soft tissue repair. The capsule, piriformis tendon, and gluteus

maximus were sequentially closed in layers with interrupted 4-0 nylon sutures. A running 4-0 nylon suture and staples were used to close the skin. Postoperative pain control was achieved with a single postoperative 0.05 mg/kg subcutaneous injection of slow-release buprenorphine, and 5 mg/kg subcutaneous injections of meloxicam daily for the first three postoperative days.

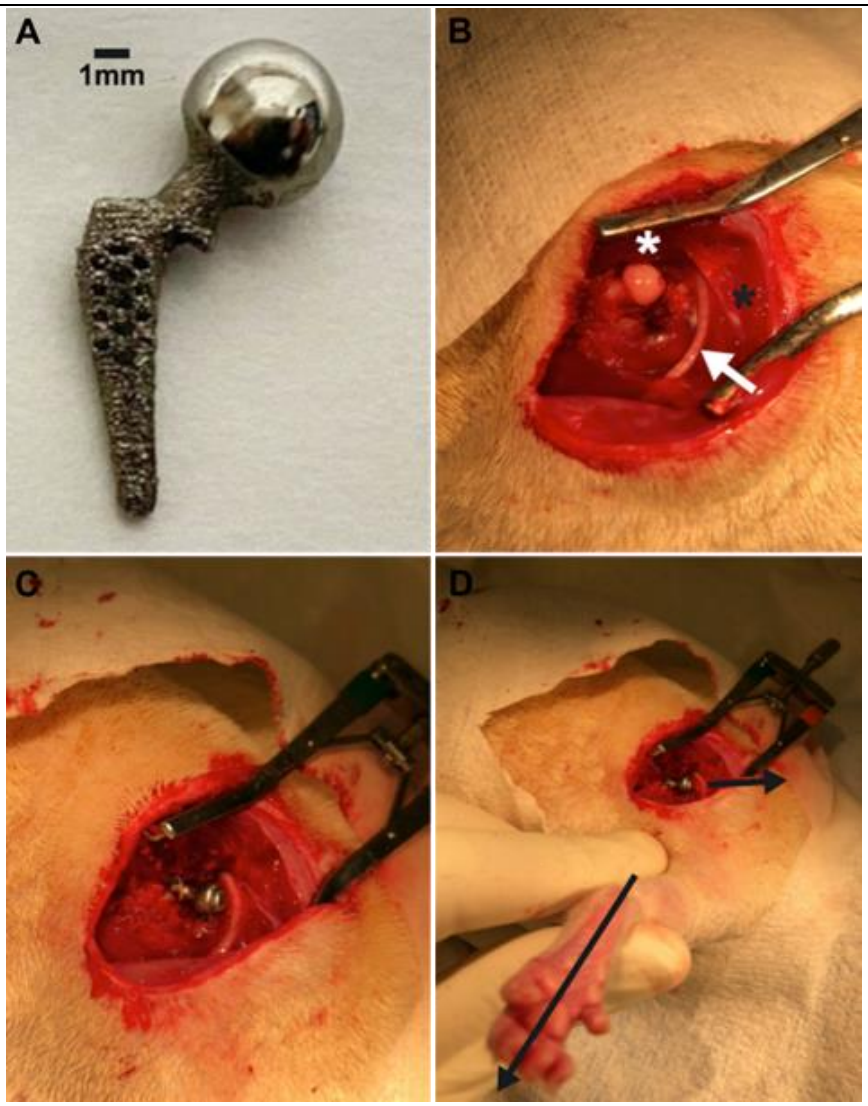

Figure 10: The Model Implant and Surgical Technique (Cementless Hip Hemiarthroplasty) A) **Model Implant** Monobloc 3D-printed, medical-grade titanium (Ti-6Al-4V) hip implants (scale=1 mm) B) **Posterior Approach** for the left hip of Sprague-Dawley rat, the hip joint is posteriorly dislocated with adduction and internal rotation of the femur after tenotomy of the piriformis and capsulotomy. Gluteus maximus (black asterisk) and Gluteus medius muscles (white asterisk) are retracted using a self-retainer retractor. Sciatic nerve (white arrows). C) **Left hip hemiarthroplasty** after replacement of the left femoral head by the hip implant D) **Femoral component version** recreating the native rat hip alignment, assessed by the thigh-foot angle (black arrows).

2.3.3 Preparation of Bacterial Inoculum

PA14-*lux* or *ΔflgK-lux* was plated on LB 1.5% agar with 20 μg/ml Gentamicin and incubated overnight at 37°C. Isolated bacterial colonies were grown at 37°C in LB broth on a roller drum at 90 rpm for 16 h. Bacterial cultures were pelleted, washed twice, and resuspended in sterile 0.9% saline. The concentration of the bacterial suspension was balanced between the 2 strains as determined by a cuvette spectrophotometer (SmartSpec™ Plus, Bio-Rad™; OD600). Bacterial load was verified by viable colony count after overnight culture on LB agar. The intraoperative contamination method to induce infection was selected since the precise number of bacteria administered is known, the method is clinically representative, and it permits investigation into how a biofilm develops on an orthopaedic implant *in vivo*.

2.3.4 Establishment of Biofilm-based GN-PJI

Preliminary experiments (N=14) were conducted to determine the optimal inoculum to induce PJI by testing intraarticular hip injection with different bacterial loads of PA14-*lux* into Sprague-Dawley rats that had undergone left hip hemiarthroplasty, after capsular closure. Intraarticular injection of 40 μl of 10^{10} CFU/ml of bacterial cell suspension (in 0.9% saline) into 2 rats resulted in development of significant hypothermia and were euthanized at postoperative day (POD) 3. Injection of 20 μl of 10^{10} CFU/ml resulted in a detectable bioluminescent signal and developed localized PJI (n=2). However, injection of 20 μl of 10^{9} and 10^{8} CFU/ml resulted in localized PJI but, bioluminescence was close to background levels (n=2). Follow up experiments (n=8) confirmed that PJI could be consistently induced by 20 μl intraarticular injection of PA14-*lux* suspension at concentration of 10^{10} CFU/ml into Sprague-Dawley rats that had undergone left hip hemiarthroplasty and the infection could be real-time monitored utilizing the *in vivo* imaging system (IVIS) PerkinElmer™.

To compare the PJI induced by PA14-*lux* versus *Δflgk-lux* strains, surgeries were performed for 3 independent cohorts. Each cohort (n=10) consisted of 3 groups: Control/Sham Surgery (hip surgery, saline injection; n=2), PA14-*lux*-PJI (hip surgery, PA14-*lux*; n=4) and *ΔflgK-lux*-PJI (hip surgery, *ΔflgK-lux*; n=4). All the rats underwent left hip hemiarthroplasty and intraarticular injection of 20 µl of sterile saline (0.9%), PA14-*lux* or *ΔflgK-lux* bacterial suspension at concentration of 10^{10} CFU/ml at the time of surgery after capsular repair. The experiments were designed first as 5 rat surgeries per day but with increased efficiency, the experiment was modified so that 10 rat surgeries were conducted per day for the 2nd and the 3rd cohorts.

2.4 Qualitative and Quantitative Assessment of PJI

2.4.1 Real-time Monitoring of PJI

Rats were anaesthetized with isoflurane and positioned in lateral decubitus with left hip up. Bioluminescence was captured with an *in vivo* imaging system (IVIS) spectrum optical imager (Caliper Life Sciences™, PerkinElmer™), at PODs 1, 2, 3, 7, 10 and 14. High-resolution images were created with color scale overlaid on a monochrome photograph of rats and quantified as total photon flux (photon/sec) of the luminescent point source in the specified region of interest (ROI) using LivingImage™ 4.7.4 software.

2.4.2 Magnetic Resonance Imaging (MRI)

MRI was conducted under general anesthesia with isoflurane at POD13, to assess the involvement of periprosthetic tissue as well as the implant position and stability, utilizing a 7T-GE/Agilent Discovery MR901 (Preclinical Imaging Core/University of Ottawa).

2.4.3 DigiGait Analysis

Gait patterns were captured with the DigiGait™ system to identify the changes before and 13 days after surgery with or without infection. Treadmill velocity was unidirectional at a constant

15cm/sec with 0° inclination. Analysis of video data was accomplished with accompanying DigiGait™ analysis software, to calculate the duration of the stance to the swing phase ratio (Stance/Swing) during the gait cycle.

2.4.4 Bacterial Load Quantification

Tissue and implant collection was performed after euthanasia at POD14. Samples were sonicated individually in a water bath for 15 min at 40 kHz (Branson™ 3510) to dislodge attached bacteria. The resulting suspensions from the sonicated implants and the homogenized periprosthetic tissue were serially diluted, then 10 µl plated on LB-agar 1.5% agar with 20 µg/ml Gentamicin, to isolate PA14-*lux* or *ΔflgK*-*lux* strains, and incubated overnight at 37°C (drop-plate method for bacterial enumeration)(Herigstad et al., 2001). Furthermore, blood, liver, kidney, spleen, and lung samples were collected, pulverized, and plated for viable colony counts.

2.4.5 Testing Osseointegration Utilizing microCT Analysis

Collected femurs, along with the retained implants, were fixed in 10% buffered formaldehyde for 10 days. Imaging MicroCT imaging (Skyscan™ 1272, Bruker™ microCT) was performed using a XIMEA xiRAY16 camera scanned at 90 kV, Cu 0.11 mm filter with a resolution image pixel size of 16 µm, over 360° and angular step 1°. 3D reconstruction was generated using NRecon™ software (version 1.7.3.1). The distal 3.2 mm of the stem was consistently selected as the region of interest (ROI). Areas of bone and implant were segmented using a region-growing algorithm for quantitative analysis of osseointegration by CTAnalyser™ (version 1.18.8.0). Bone contact was measured at 10 pixels dilation selected 5 pixels away from the metal implant surface, due to the density artefacts that affect the microCT cross-sectional images in the immediate vicinity of the metal surface. Intersection surface (IS) is measured and corresponds to the bone-to-implant contact (BIC).

2.4.6 Field-Emission Scanning Electron Microscopy (FE-SEM)

Femurs were decalcified using formic acid (10%) before removal of the retained implants, ensuring maintenance of the structure of bone-implant-interface. Implants were dried with TSAMDRI-PVT-3D (Tousimis™) critical-point-dryer, then coated with 6-8nm of gold using a LEICA EM ACE200 vacuum-coater (Leica™ Microsystems). Bacterial colonization and biofilm formation at the interface was scanned with a JEOL, JSM-7500F FE-SEM (JEOL™) at 10 kV and variable magnification.

2.5 Statistical analysis

For descriptive statistics, continuous variables were reported as mean, standard deviation and range. Bacterial loads between 2 infection groups were compared using independent-samples t-tests. Postoperative Stance/Swing compared to preoperative were analyzed using paired t-tests. One-way ANOVA was utilized to compare IS between the 3 experimental groups with Tukey multiple comparison test. With 95% confidence intervals, p-value<0.05 was considered significant. All analyses were performed using GraphPad Prism v.8.0.0 for Windows (GraphPad™ Software, USA). For our *post hoc* power analysis, a sample size of 8 rats allowed the detection of an effect size of $2.5x10^6$ P/sec between groups, with a 0.05 level of significance and power of 0.80. sample size of 8 rats allowed the detection of an effect size of 1.16 in Stance/Swing before and after surgery, with a 0.05 level of significance and power of 0.80 and a sample size of 9 rats allowed the detection of an effect size of $2.65x10^6$ μm^2 in intersection surface between groups, with a 0.05 level of significance and power of 0.80.

CHAPTER 3: RESULTS

3.1 Evaluating Systemic Response to GN-PJI

Systemic response to infection was indirectly assessed by regular measurements of weight and temperature at PODs 0, 1, 2, 3, 7, 10 and 14. Gradual, subtle weight loss in the 3 groups was the earliest and most reliable sign of systemic deterioration during the first week in response to surgery. However, all rats started to regain weight during the second week (Figure 11A). Spikes of fever were observed during the first 3 PODs in both infected groups. However, the temperature was stable for all groups during the second week confirming that the rats did not develop systemic sepsis (Figure 11B). Moreover, no bacteria could be isolated from the blood, liver, spleen, kidney, or lung samples for any of the groups, suggesting a localized, walled-off implant related infection with no systemic dissemination.

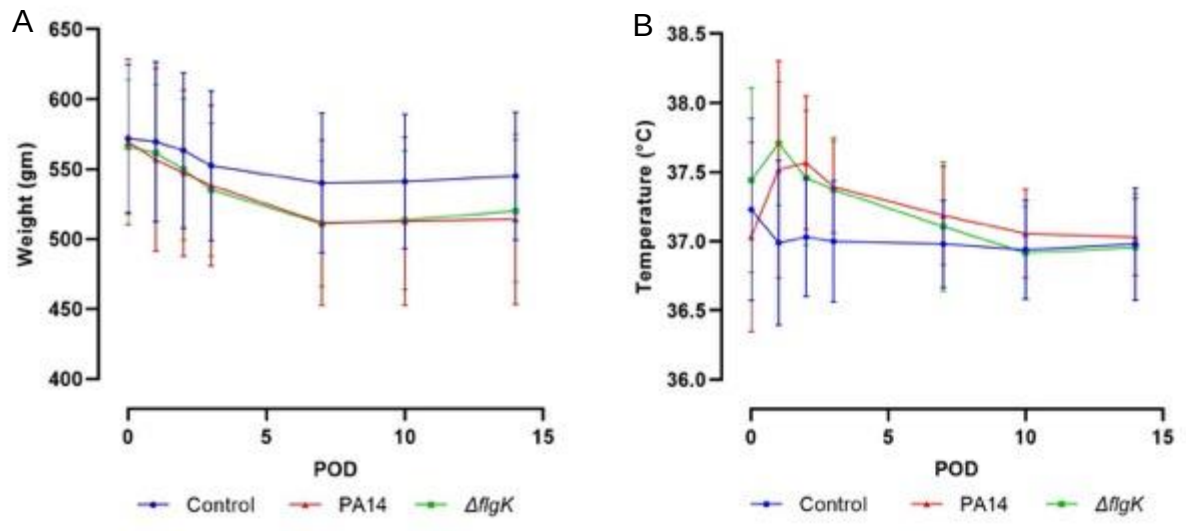

Figure 11: Systemic response to infection (Clinical outcome)
A) Weight and B) Temperature measurement at PODs 0, 1, 2, 3, 7, 10 and 14 for PA14-*lux*-PJI, *ΔflgK*-*lux*-PJI versus non-infected surgical control groups. Error bars are the standard deviation of the mean. (PODs Post-Operative Days)

3.2 Evaluation of Biofilm Formation and Periprosthetic Tissue:

3.2.1 Real-time Monitoring of PJI *(in vivo)*

Infection was reliably established within the hip joint and was followed by IVIS in real-time. Bioluminescence signal intensity for the 2 infected groups peaked 3-days postoperatively and waned gradually till the endpoint. Despite the inherent variability of this model system, I observed the persistence of higher signal intensity for the PJI group induced by PA14-*lux* (n=8) versus the *ΔflgK*-*lux*-PJI group (n=8) compared to the non-infected surgical control group (n=4) (Figure 12). The bioluminescence signal was focused on the hip region, demonstrating a localized infection.

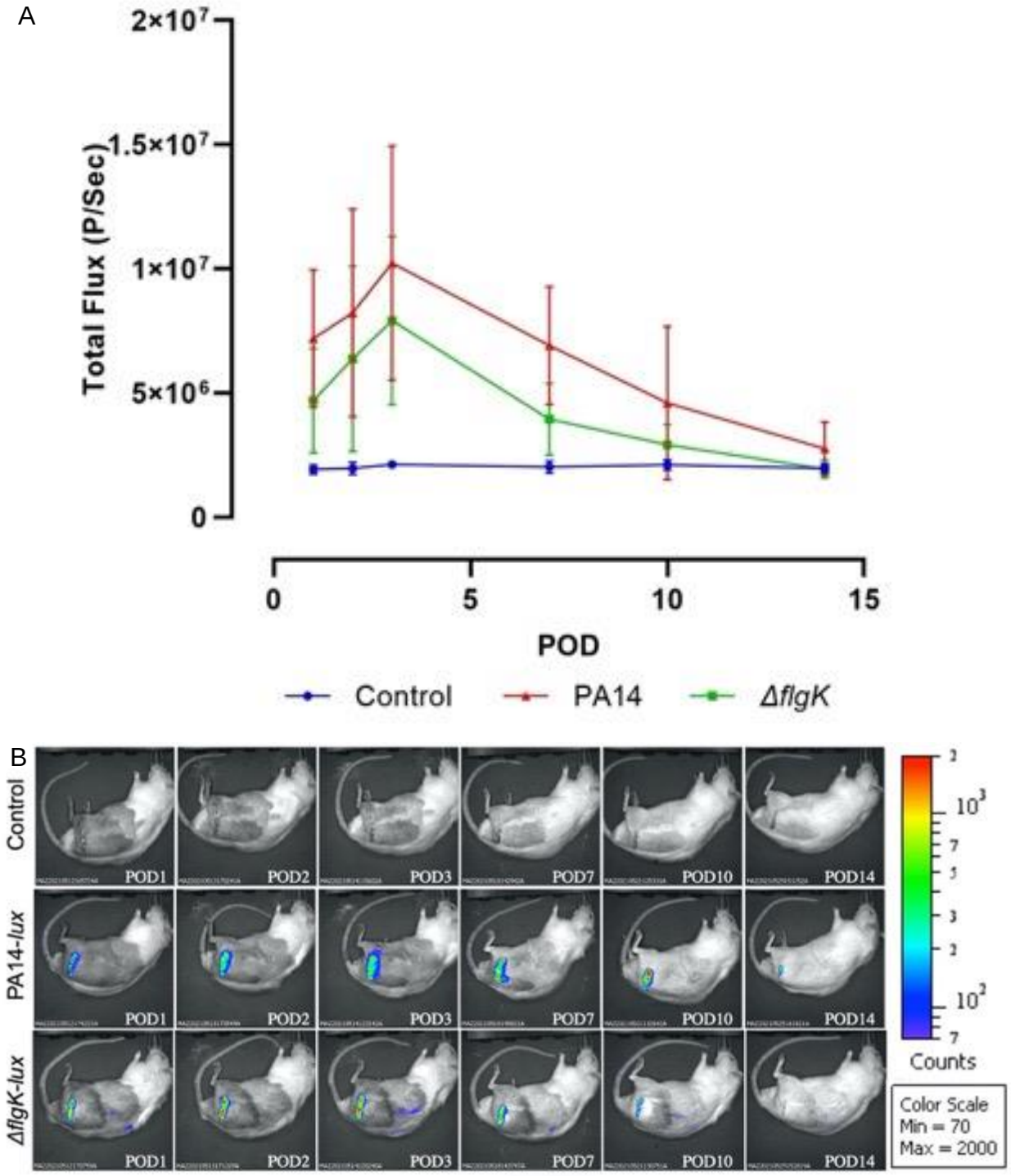

Figure 12: *In vivo* Imaging System (IVIS) A) Plotting the bioluminescence signal intensity, total photon flux (P/Sec) of the luminescent point source in the specified ROI(s). The depicted curve is the mean value of 8 biologic replicates from each group of PJI induced by PA14-*lux* or *ΔflgK*-*lux* and 4 biologic replicates of the non-infected surgical control to identify the limit of detection. Error bars are the standard deviation of the mean. B) Composite images generated by LivingImage™ 4.7.4 software.

3.2.2 Bacterial Load (*in vitro*)

For quantitative assessment of biofilm formation, the bacterial load was quantified by viable colony count of the living bacterial cells in the biofilm attached to implant surface and within the collected periprosthetic tissues. Analysis of bacteria associated with the implants showed a statistically significant reduction in the bacterial loads associated with implants from the *ΔflgK*-*lux*-PJI group (n=12) versus the PA14-*lux*-PJI group (n=16), with no bacteria associated with the non-infected surgical control group (n=10); p=0.016. There was no statistically significant difference in the bacterial loads associated with the homogenized periprosthetic tissues between the 2 groups (Figure 13).

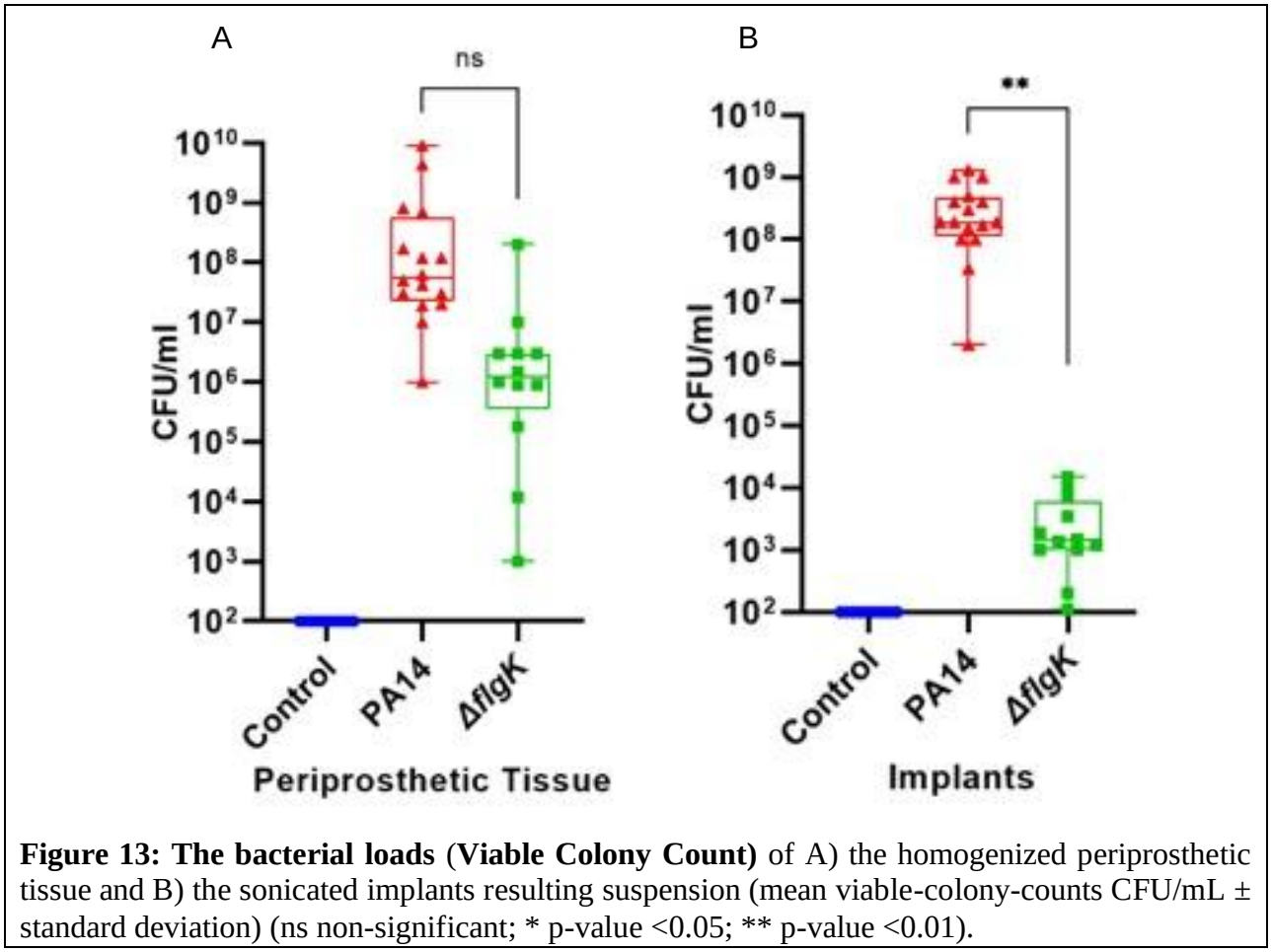

Figure 13: The bacterial loads (**Viable Colony Count)** of A) the homogenized periprosthetic tissue and B) the sonicated implants resulting suspension (mean viable-colony-counts CFU/mL ± standard deviation) (ns non-significant; * p-value <0.05; ** p-value <0.01).

3.2.3 MRI (*in vivo*)

To assess the involvement of periprosthetic tissues in response to PJI *in vivo* as well as the implant position and stability, MRI was acquired at POD 13 under general anesthesia. PJI induced by PA14-*lux* was characterized by the formation of a large abscess. A relatively smaller abscess induced by *ΔflgK-lux*. The MRI images ensured the implants' stability in position with the stem inside the femoral canal and the head articulating with the acetabulum (Figure 14).

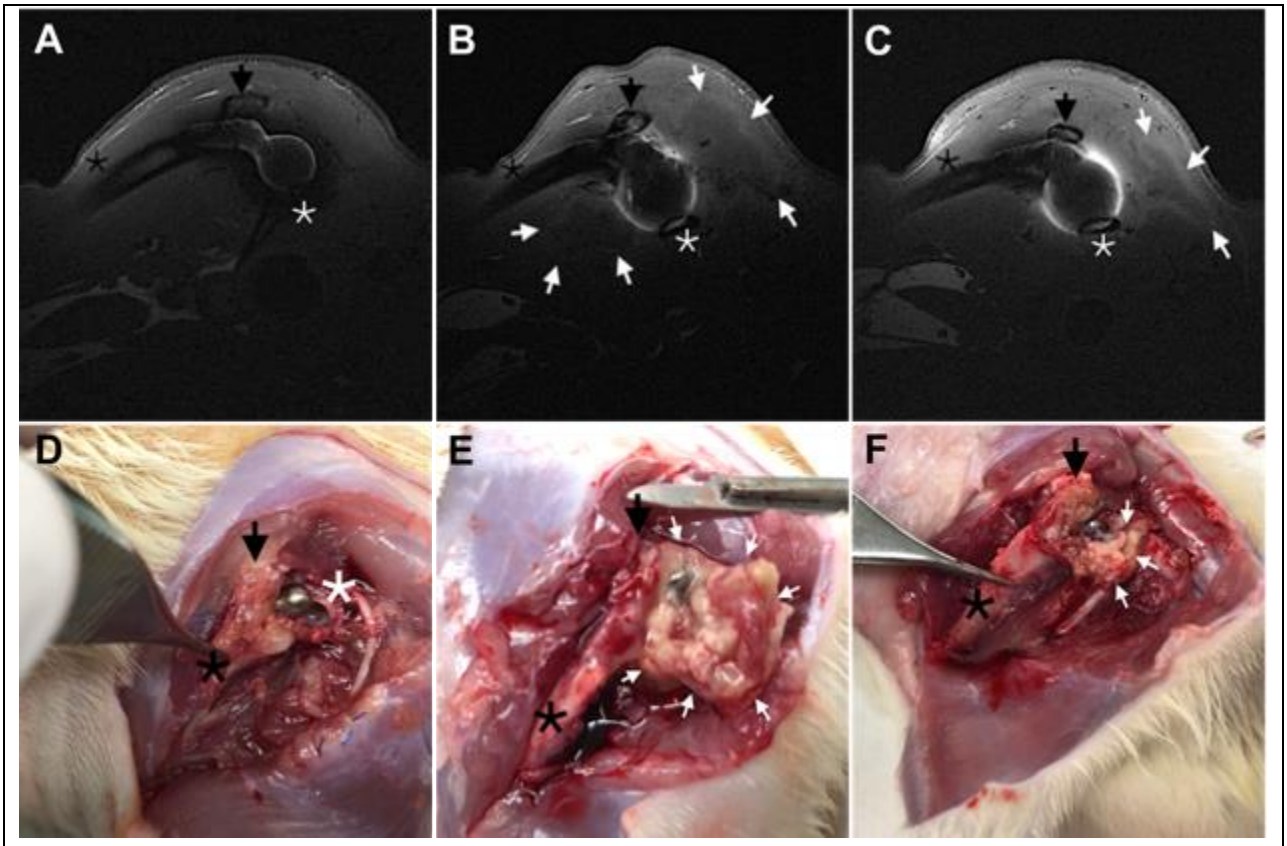

Figure 14: Representative sections of left hip MRI for A) a non-infected surgical control (n=2), B) PA14-*lux*-PJI (n=3) demonstrating periprosthetic abscess (white arrows) and C) *ΔflgK-lux*-PJI (n=3) with a relatively smaller abscess (white arrows). The MRI images demonstrated stable implants in position with the stem inside the femoral canal (black asterisk) and the head articulating with the acetabulum (white asterisk). Greater Trochanter (black arrow).
Corresponding representative images post euthanasia during dissection, implant and periprosthetic tissue collection for D) a non-infected surgical control, E) PA14-*lux*-PJI and F) *ΔflgK-lux*-PJI, with similar findings correlated with the MRI images.

3.2.4 FE-SEM (*in vitro*)

FE-SEM was utilized to visually confirm the biofilm formation at the bone-implant-interface in response to PJI induced by different PA strains. Scanning of the bone-implant-interface of PA14-*lux*-PJI group demonstrated the bacilli encased in biofilm versus few individual surface-attached cells with defective biofilm formation in the *ΔflgK-lux*-PJI group (Figure 15)

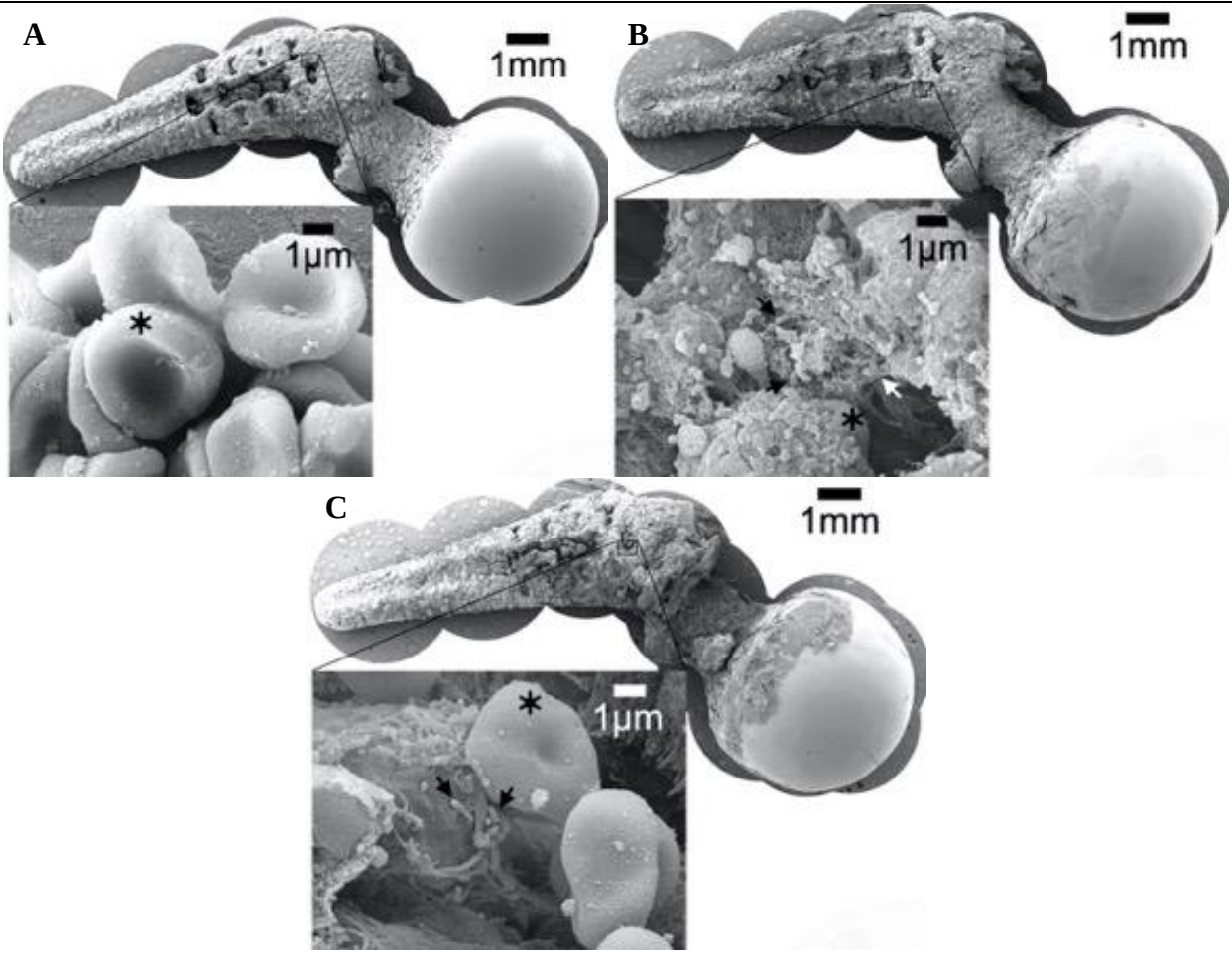

Figure 15: FE-SEM imaging of explanted implants (25x magnification; scale bar =1 mm) at the bone-implant-interface (inset image 10k x magnification; scale bar =1 µm) of A) non-infected surgical control (n=2), B) PA14-*lux*-PJI group (n=2), demonstrating the bacilli (black arrows) encased in biofilm (white arrow) versus C) *ΔflgK-lux*-PJI (n=2), with individual bacilli (black arrows) with no extracellular matrix. Host cells e.g., RBCs (black asterisk).

3.3 Evaluation of the Implant Stability and Function

The implant stability, as an outcome, was directly assessed by quantifying the osseointegration *in vitro* using microCT scan, and indirectly assessed by identifying the gait pattern changes using DigiGait™ system *in vivo*.

3.3.1 DigiGait Analysis (*in vivo*)

The DigiGait™ system measurements showed a statistically significant reduction in the postoperative Stance/Swing ratio of PA14-*lux*-PJI group (n=15; *p*=0.0012; 95% CI: -2.683 to -0.8236) relative to preoperative ratio with less significant reduction for the *ΔflgK*-*lux*-PJI group (n=11; *p*=0.0159; 95% CI: -2.219 to -0.2901) and non-significant reduction for the non-infected surgical control group (n=8; *p*=0.2883; 95% CI: –2.370 to 0.8199) (Figure 16).

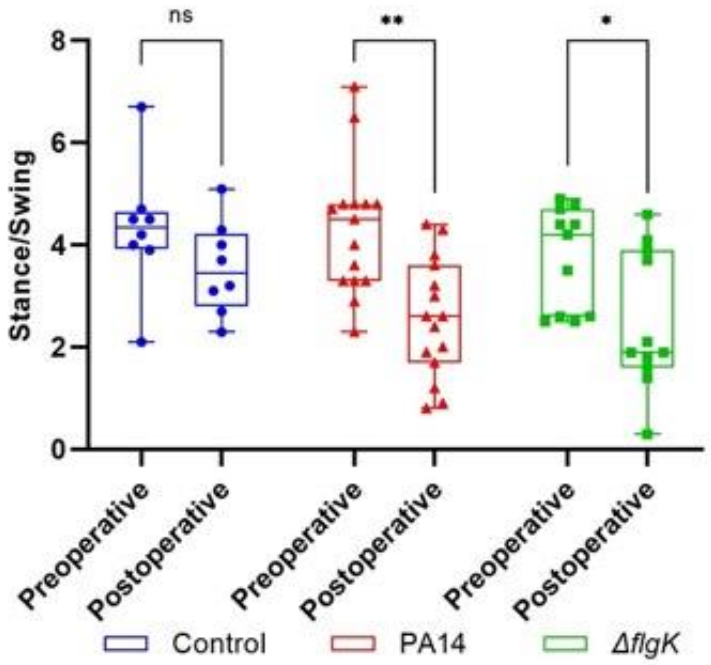

Figure 16: Weight-bearing and gait pattern analysis captured with the DigiGait™ system A box plot to compare postoperative relative to preoperative Stance/Swing ratio of the non-infected surgical control (n=8), PA14-*lux*-PJI (n=15) and *ΔflgK*-*lux*-PJI (n=11) groups (ns non-significant; * p-value <0.05; ** p-value <0.01).

3.3.2 Testing Osseointegration Utilizing microCT Analysis (*in vitro*)

Analysis of the BIC at the distal end of the implant showed a statistically significant lower IS of PA14-*lux*-PJI group (n=9) compared to *ΔflgK*-*lux*-PJI (n=9) and the non-infected surgical control groups (n=5) p=0.048 (Figure 17).

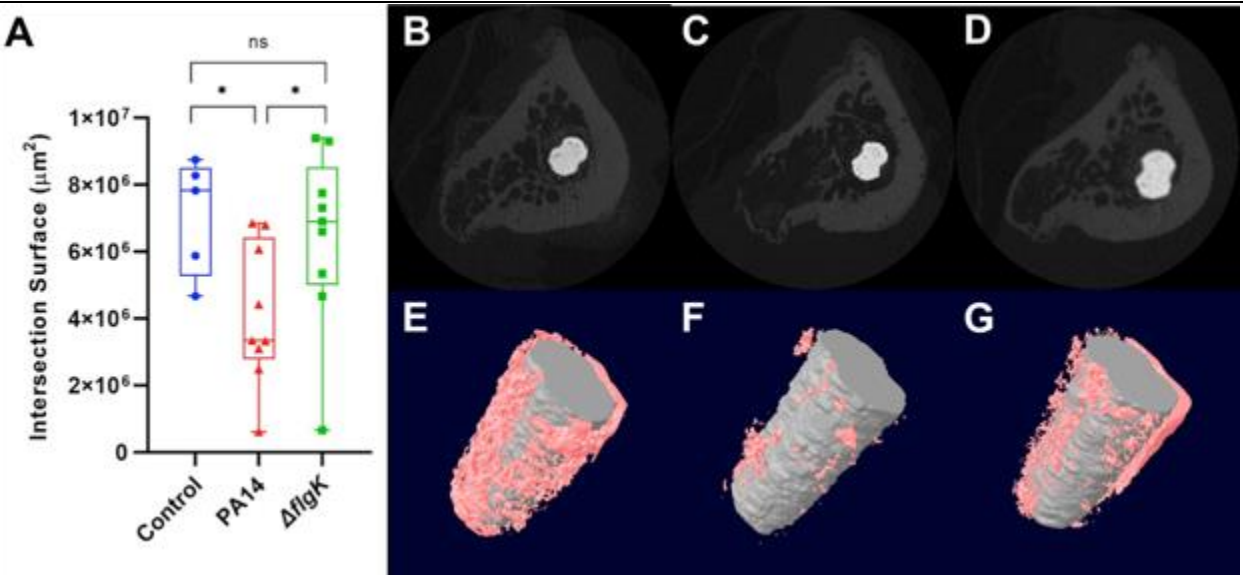

Figure 17: Testing osseointegration utilizing microCT scanning of the collected femurs with retained implants A) A box plot demonstrating bone to implant contact (BIC) at the distal end of the implant by Intersection Surface (IS) of PA14-*lux*-PJI (n=9) group (C, F) compared to *ΔflgK*-*lux*-PJI (n=9) (D, G) and the non-infected surgical control (n=5) groups (B, E). CT images on top (B, C, D) and quantified by the corresponding 3D model below (E, F, G).

CHAPTER 4: DISCUSSION

Despite recent clinical focus on prevention and treatment of PJI, no significant improvement in outcomes has been observed (Alamanda and Springer, 2019; Jämsen et al., 2009). Several decades of research have contributed to building the foundation for developing *in vitro* and *in vivo* biofilm PJI models (Bernthal et al., 2010; Carli et al., 2016, 2017; Craig et al., 2005; Hadden et al., 2021; Li et al., 2008; Lovati et al., 2017; Nijhof et al., 2000; Niska et al., 2012; Poultsides et al., 2008; Premkumar et al., 2021b; Pribaz et al., 2012; Thompson et al., 2018), each one with its own characteristics, uses, advantages, and limitations (Guzmán-Soto et al., 2021). Over the last decade, there has been a push to develop new *in vivo* biofilm models that address the shortcomings of available models and to reliably test novel therapeutics. The current study proposes a novel, clinically representative, biofilm-based *in vivo* GN-PJI model. This model provided quantitative correlation between biofilm formation and implant osseointegration. This correlation was demonstrated directly by microCT and indirectly by the significant decline of the Stance/Swing ratio of the PA14-*lux* induced PJI assessed by DigiGait analysis compared to the biofilm defective mutant *ΔflgK-lux* and the non-infected surgical control.

Unlike *in vitro* models where the biofilm is accessible and its development can be easily monitored, assessing biofilm formation *in vivo* is more challenging, and typically is carried out postmortem. The current model utilizes bioluminescent PA strains (PA14-*lux* and *ΔflgK-lux*) to induce PJI. To insert the *lux* operon, I chose the mini-Tn7 system because it is easy and efficient to use. It allows site- and orientation-specific chromosomal insertion at a predictable neutral *att*-site, so it avoids the necessity for continued antibiotic selection, making it ideal for animal models,

especially if therapeutics are to be tested (Choi and Schweizer, 2006; Choi et al., 2005). This system has broad host-range capabilities (Choi and Schweizer, 2006; Choi et al., 2005; Craig, 1996), so it can be utilized with different species or clinical isolates for *in vivo* testing. This study has introduced the MRI, as a successful non-invasive modality to demonstrate PJI associated abscess formation for *in vivo* monitoring.

Powers et al (Powers et al., 1995) first piloted THA in rats, however no subsequent hip PJI *in vivo* model has been developed, most likely due to the complexity of the procedure, especially with the cup component insertion. Cemented hip hemiarthroplasty PJI model has been reported, but it is limited in its ability to test effect of infection on osseointegration (Hadden et al., 2021). Subsequently, cementless hip implant was selected for this model, with the topographic features allowing osseointegration and insertion technique recapitulating the press-fit mode of fixation utilized in clinical setting. A posterior approach to the hip joint was performed as described by Hadden *et al* (Hadden et al., 2021) to maintain the abductor function and preserve hip biomechanics (Hadden et al., 2021). The results were corroborated by the DigiGait analysis data. Meticulous repair of the capsule and piriformis tendon also allowed hip joint stability. Only 1 hip dislocation (2%) was reported.

Interestingly, bacterial colonization and biofilm formation at the bone implant interface was demonstrated by the FE-SEM at 2 weeks of infection. This finding might be a good reason to re-evaluate the current classifications of PJI in order to guide the treatment (Haddad and Bridgens, 2008). Traditional definition for early PJI has been proposed by Infectious Diseases Society of America (IDSA) was less than 3 months after surgery (Zimmerli et al., 2004). Another novel

classification defined acute hematogenous PJI less than 3 of weeks duration and early postinterventional PJI when infection occurs within 1 month after implantation. Early PJI generally could be treated with debridement antibiotic and implant retention (DAIR). By contrast, in patients with a chronic PJI, the biofilm adhering to the implant generally cannot be eliminated by antimicrobial agents or mechanical debridement (Davies, 2003; Guzmán-Soto et al., 2021; Hall and Mah, 2017; Mah and O'Toole, 2001; Nickel et al., 1985; O'Toole et al., 2000; Olsen, 2015; Premkumar et al., 2021b; Stoodley et al., 2011) Therefore, the implant has to be removed and/or replaced (Tsukayama et al., 1996; Zimmerli, 2014). Novel treatment strategies and techniques are certainly needed as current strategies remain far from optimal, with no substantial improvement in the treatment success rates of PJI could be observed (Xu et al., 2020).

The main strength of this study is its translational relevance; as I relied on diverse of methodologies to assess PJI and quantify biofilm formation *in vivo* such as IVIS and MRI, and *in vitro* such as viable colony count of the bacterial load and FE-SEM of the collected implants and periprosthetic tissues. However, this study does have limitations. First, healthy animals were used whereas patients who need arthroplasty typically have associated comorbidities such as obesity or diabetes. For instance, one study demonstrated that diabetic mice had impaired wound healing and were more prone to PA infection, compared to nondiabetics (Lazurko et al., 2020). Second, a much higher bacterial concentration (10^{10} CFU/ml) for the inoculum was utilized, compared to the exposure that typically occurs clinically (~100 CFUs/ml)(Stocks et al., 2011). However, similarly high bacterial concentrations have been utilized with other models in the literature (Petty et al., 1985, 1988; Poultsides et al., 2008) and to the chosen concentration allowed me to monitor the biofilm development *in vivo* using the IVIS. We observed from our previous analyses (preliminary

experiments as well as the published cemented model (Hadden et al., 2021)) that the bioluminescent signal could not be consistently detectable with the lower doses. Moreover, biofilm assessment was challenging to perform *in vivo* using the FE-SEM because of the host tissue attached to the explanted implants. Finally, the osseointegration was tested using only the microCT without pullout strength, as pulling the implant out of the femur could disturb the implant surface biofilm.

Almost all the rats tolerated the procedure. There were 2 exceptions (4%). These rats developed apnea immediately after surgery, most likely, because of the respiratory depression side effect of the slow-release buprenorphine (0.05 mg/kg) subcutaneously, combined with the isoflurane inhalation (Criado et al., 2000). To improve the safety, the analgesia protocol was modified by administrating only half dose of slow-release buprenorphine preoperatively, and the remaining half during the recovery. One of the non-infected surgical controls (2%) suffered an implant stem fatigue fracture while the distal segment of the stem was securely fixed in the femoral canal. This created the bending cantilever fatigue mode of failure (Gruen et al., 1979). Avulsion fractures of the greater trochanter and lesser trochanter were observed in 2 rats of the PA14-*lux*-PJI group, most likely because of significant periprosthetic osteolysis (Figure 18). Chen et al recently reported the lipopolysaccharide (LPS) mediated osteoclast differentiation adverse effects on bone in a setting of GN-PJI (Chen et al., 2019). Despite these complications, the proposed rat model is unique in its ability to translate important clinical features associated with GN-PJI. This model can be utilized to provide a better understanding of GN biofilm pathogenesis and for testing novel biofilm-targeting therapeutics.

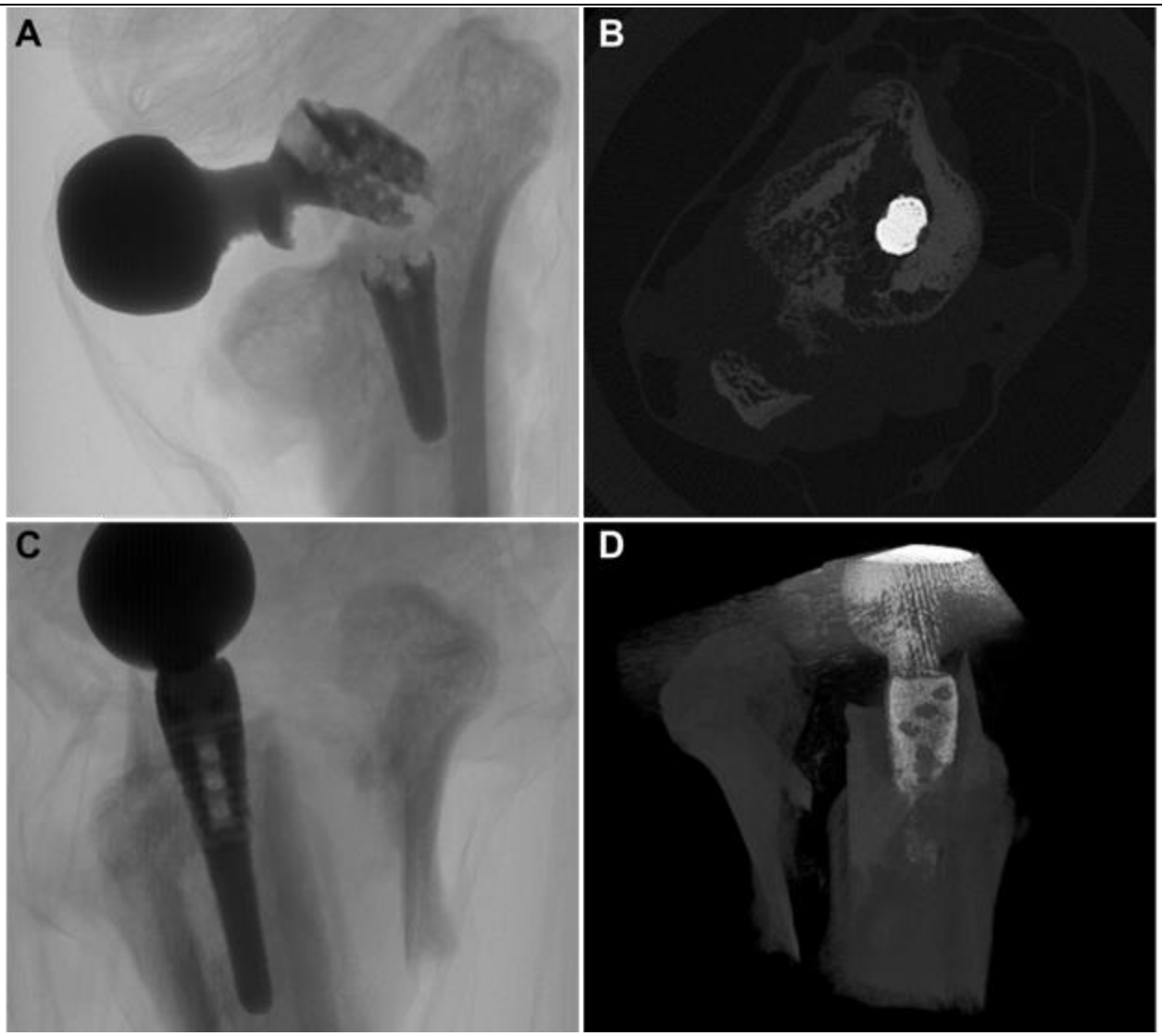

Figure 18: Complications A) X-ray of left proximal femur of the non-infected surgical control group in anteroposterior (AP) projection showing stem fracture B) Axial slice of left proximal femur of one rat of the PA14-*lux*-PJI group is showing lesser trochanter avulsion fracture. C) X-ray of left proximal femur of one rat of the PA14-*lux*-PJI group in lateral projection and, D) 3D reconstruction, are showing greater trochanter avulsion fracture.

In conclusion, I developed a novel uncemented hip hemiarthroplasty GN-PJI rat model. This model is clinically-representative since animals can bear weight on the implant, successfully reproduces the periprosthetic environment consisting of the hypovascular (immune-privileged) articular space, hypercellular intramedullary space, and the arthroplasty implant that separates the 2 environments. PJI was detected by various modalities. In addition, biofilm formation correlated with implant function and stability. The proposed model will allow for insights GN biofilm formation pathogenesis and more reliable testing of novel biofilm-targeting therapeutics.

LIST OF REFERENCES

Abe, R., Oda, S., Sadahiro, T., Nakamura, M., Hirayama, Y., Tateishi, Y., Shinozaki, K., and Hirasawa, H. (2010). Gram-negative bacteremia induces greater magnitude of inflammatory response than Gram-positive bacteremia. Crit. Care *14*, R27.

Abouljoud, M.M., Backstein, D., Battenberg, A., Dietz, M., Erice, A., Freiberg, A.A., Granger, J., Katchky, A., Khlopas, A., Kim, T.-K., et al. (2019). Hip and Knee Section, Treatment, Surgical Technique: Proceedings of International Consensus on Orthopedic Infections. J. Arthroplasty *34*, S445–S451.

Akindolire, J., Morcos, M.W., Marsh, J.D., Howard, J.L., Lanting, B.A., and Vasarhelyi, E.M. (2020). The economic impact of periprosthetic infection in total hip arthroplasty. Can. J. Surg. *63*, E52–E56.

Alamanda, V.K., and Springer, B.D. (2019). The prevention of infection: 12 modifiable risk factors. Bone Joint J. *101-B*, 3–9.

Alm, R.A., and Mattick, J.S. (1995). Identification of a gene, pilV, required for type 4 fimbrial biogenesis in *Pseudomonas aeruginosa*, whose product possesses a pre-pilin-like leader sequence. Mol. Microbiol. *16*, 485–496.

Alm, R.A., Hallinan, J.P., Watson, A.A., and Mattick, J.S. (1996). Fimbrial biogenesis genes of *Pseudomonas aeruginosa*: *pilW* and *pilX* increase the similarity of type 4 fimbriae to the GSP protein-secretion systems and *pilY1* encodes a gonococcal *PilC* homologue. Mol. Microbiol. *22*, 161–173.

Anagnostakos, K., and Meyer, C. (2019). Partial two-stage exchange at the site of periprosthetic hip joint infections. Arch. Orthop. Trauma Surg. *139*, 869–876.

Armstrong, M.D., Carli, A. V, Abdelbary, H., Poitras, S., Lapner, P., and Beaule, P.E. (2018).

Tertiary care centre adherence to unified guidelines for management of periprosthetic joint infections: a gap analysis. Can. J. Surg. *61*, 34–41.

Baldoni, D., Haschke, M., Rajacic, Z., Zimmerli, W., and Trampuz, A. (2009). Linezolid alone or combined with rifampin against methicillin-resistant *Staphylococcus aureus* in experimental foreign-body infection. Antimicrob. Agents Chemother. *53*, 1142–1148.

Barken, K.B., Pamp, S.J., Yang, L., Gjermansen, M., Bertrand, J.J., Klausen, M., Givskov, M., Whitchurch, C.B., Engel, J.N., and Tolker-Nielsen, T. (2008). Roles of type IV pili, flagellum-mediated motility and extracellular DNA in the formation of mature multicellular structures in *Pseudomonas aeruginosa* biofilms. Environ. Microbiol. *10*, 2331–2343.

Belmatoug, N., Crémieux, A.C., Bleton, R., Volk, A., Saleh-Mghir, A., Grossin, M., Garry, L., and Carbon, C. (1996). A new model of experimental prosthetic joint infection due to methicillin-resistant *Staphylococcus aureus*: a microbiologic, histopathologic, and magnetic resonance imaging characterization. J. Infect. Dis. *174*, 414–417.

Benito, N., Franco, M., Coll, P., Gálvez, M.L., Jordán, M., López-Contreras, J., Pomar, V., Monllau, J.C., Mirelis, B., and Gurguí, M. (2014). Etiology of surgical site infections after primary total joint arthroplasties. J. Orthop. Res. Off. Publ. Orthop. Res. Soc. *32*, 633–637.

Benito, N., Franco, M., Ribera, A., Soriano, A., Rodriguez-Pardo, D., Sorli, L., Fresco, G., Fernandez-Sampedro, M., Dolores Del Toro, M., Guio, L., et al. (2016). Time trends in the aetiology of prosthetic joint infections: a multicentre cohort study. Clin. Microbiol. Infect. Off. Publ. Eur. Soc. Clin. Microbiol. Infect. Dis. *22*, 732.e1-8.

de Bentzmann, S., Giraud, C., Bernard, C.S., Calderon, V., Ewald, F., Plésiat, P., Nguyen, C., Grunwald, D., Attree, I., Jeannot, K., et al. (2012). Unique biofilm signature, drug susceptibility and decreased virulence in *Drosophila* through the *Pseudomonas aeruginosa* two-component

system PprAB. PLoS Pathog. *8*, e1003052.

Bernthal, N.M., Stavrakis, A.I., Billi, F., Cho, J.S., Kremen, T.J., Simon, S.I., Cheung, A.L., Finerman, G.A., Lieberman, J.R., Adams, J.S., et al. (2010). A mouse model of post-arthroplasty *Staphylococcus aureus* joint infection to evaluate *in vivo* the efficacy of antimicrobial implant coatings. PLoS One *5*, e12580.

Beswick, A.D., Elvers, K.T., Smith, A.J., Gooberman-Hill, R., Lovering, A., and Blom, A.W. (2012). What is the evidence base to guide surgical treatment of infected hip prostheses? systematic review of longitudinal studies in unselected patients. BMC Med. *10*, 18.

Bozic, K.J., and Ries, M.D. (2005). The impact of infection after total hip arthroplasty on hospital and surgeon resource utilization. J. Bone Joint Surg. Am. *87*, 1746–1751.

Brandt, C.M., Sistrunk, W.W., Duffy, M.C., Hanssen, A.D., Steckelberg, J.M., Ilstrup, D.M., and Osmon, D.R. (1997). *Staphylococcus aureus* prosthetic joint infection treated with debridement and prosthesis retention. Clin. Infect. Dis. an Off. Publ. Infect. Dis. Soc. Am. *24*, 914–919.

Caiazza, N.C., and O'Toole, G.A. (2004). SadB is required for the transition from reversible to irreversible attachment during biofilm formation by *Pseudomonas aeruginosa* PA14. J. Bacteriol. *186*, 4476–4485.

Carli, A. V, Ross, F.P., Bhimani, S.J., Nodzo, S.R., and Bostrom, M.P.G. (2016). Developing a Clinically Representative Model of Periprosthetic Joint Infection. J. Bone Joint Surg. Am. *98*, 1666–1676.

Carli, A. V, Bhimani, S., Yang, X., Shirley, M.B., de Mesy Bentley, K.L., Ross, F.P., and Bostrom, M.P.G. (2017). Quantification of Peri-Implant Bacterial Load and *in Vivo* Biofilm Formation in an Innovative, Clinically Representative Mouse Model of Periprosthetic Joint Infection. JBJS *99*.

Castañeda, S., Largo, R., Calvo, E., Rodríguez-Salvanés, F., Marcos, M.E., Díaz-Curiel, M., and

Herrero-Beaumont, G. (2006). Bone mineral measurements of subchondral and trabecular bone in healthy and osteoporotic rabbits. Skeletal Radiol. *35*, 34–41.

Cerioli, M., Batailler, C., Conrad, A., Roux, S., Perpoint, T., Becker, A., Triffault-Fillit, C., Lustig, S., Fessy, M.-H., Laurent, F., et al. (2020). *Pseudomonas aeruginosa* Implant-Associated Bone and Joint Infections: Experience in a Regional Reference Center in France. Front. Med. *7*, 513242.

Chen, M.-F., Chang, C.-H., Hu, C.-C., Wu, Y.-Y., Chang, Y., and Ueng, S.W.N. (2019). Periprosthetic Joint Infection Caused by Gram-Positive Versus Gram-Negative Bacteria: Lipopolysaccharide, but not Lipoteichoic Acid, Exerts Adverse Osteoclast-Mediated Effects on the Bone. J. Clin. Med. *8*.

Choi, K.-H., and Schweizer, H.P. (2006). mini-Tn7 insertion in bacteria with single *attTn7* sites: example *Pseudomonas aeruginosa*. Nat. Protoc. *1*, 153–161.

Choi, K.-H., Gaynor, J.B., White, K.G., Lopez, C., Bosio, C.M., Karkhoff-Schweizer, R.R., and Schweizer, H.P. (2005). A Tn7-based broad-range bacterial cloning and expression system. Nat. Methods *2*, 443–448.

Christensen, G.D., Simpson, W.A., Younger, J.J., Baddour, L.M., Barrett, F.F., Melton, D.M., and Beachey, E.H. (1985). Adherence of coagulase-negative *staphylococci* to plastic tissue culture plates: a quantitative model for the adherence of *staphylococci* to medical devices. J. Clin. Microbiol. *22*, 996–1006.

CIHI (2019). Canadian Institute for Health Information; Hip and Knee Replacements in Canada, 2017–2018: Canadian Joint Replacement Registry Annual Report (Ottawa ON).

Ciofu, O., Rojo-Molinero, E., Macia, M.D., and Oliver, A. (2017). Antibiotic treatment of biofilm infections. APMIS *125*, 304–319.

Cohen, J. (2001). Mechanisms of tissue injury in sepsis: contrasts between gram positive and gram

negative infection. J. Chemother. *13 Spec No*, 153–158.

Convery, F.R. (1992). Hip arthroplasty. Edited By H. C. Amstutz. New York: Churchill Livingstone, 1991. 1,001 pp, 195. J. Orthop. Res. *10*, 601.

Corvec, S., Furustrand Tafin, U., Betrisey, B., Borens, O., and Trampuz, A. (2013). Activities of fosfomycin, tigecycline, colistin, and gentamicin against extended-spectrum-β-lactamase-producing *Escherichia coli* in a foreign-body infection model. Antimicrob. Agents Chemother. *57*, 1421–1427.

Craig, N.L. (1996). Transposon Tn7. Curr. Top. Microbiol. Immunol. *204*, 27–48.

Craig, M.R., Poelstra, K.A., Sherrell, J.C., Kwon, M.S., Belzile, E.L., and Brown, T.E. (2005). A novel total knee arthroplasty infection model in rabbits. J. Orthop. Res. Off. Publ. Orthop. Res. Soc. *23*, 1100–1104.

Criado, A.B., Gómez de Segura, I.A., Tendillo, F.J., and Marsico, F. (2000). Reduction of isoflurane MAC with buprenorphine and morphine in rats. Lab. Anim. *34*, 252–259.

Cunningham, D.J., Kavolus, J.J. 2nd, Bolognesi, M.P., Wellman, S.S., and Seyler, T.M. (2017). Specific Infectious Organisms Associated With Poor Outcomes in Treatment for Hip Periprosthetic Infection. J. Arthroplasty *32*, 1984-1990.e5.

Davies, D. (2003). Understanding biofilm resistance to antibacterial agents. Nat. Rev. Drug Discov. *2*, 114–122.

Davies, D.G., and Geesey, G.G. (1995). Regulation of the alginate biosynthesis gene algC in *Pseudomonas aeruginosa* during biofilm development in continuous culture. Appl. Environ. Microbiol. *61*, 860–867.

Davies, D.G., Chakrabarty, A.M., and Geesey, G.G. (1993). Exopolysaccharide production in biofilms: substratum activation of alginate gene expression by *Pseudomonas aeruginosa*. Appl.

Environ. Microbiol. *59*, 1181–1186.

Diard, M., Baeriswyl, S., Clermont, O., Gouriou, S., Picard, B., Taddei, F., Denamur, E., and Matic, I. (2007). *Caenorhabditis elegans* as a simple model to study phenotypic and genetic virulence determinants of extraintestinal pathogenic *Escherichia coli*. Microbes Infect. *9*, 214–223.

Doeing, D.C., Borowicz, J.L., and Crockett, E.T. (2003). Gender dimorphism in differential peripheral blood leukocyte counts in mice using cardiac, tail, foot, and saphenous vein puncture methods. BMC Clin. Pathol. *3*, 3.

Egermann, M., Goldhahn, J., and Schneider, E. (2005). Animal models for fracture treatment in osteoporosis. Osteoporos. Int. a J. Establ. as Result Coop. between Eur. Found. Osteoporos. Natl. Osteoporos. Found. USA *16 Suppl 2*, S129-38.

El-Husseiny, M., and Haddad, F.S. (2016). The Role of Highly Selective Implant Retention in the Infected Hip Arthroplasty. Clin. Orthop. Relat. Res. *474*, 2157–2163.

Fagotti, L., Tatka, J., Salles, M.J.C., and Queiroz, M.C. (2018). Risk Factors and Treatment Options for Failure of a Two-Stage Exchange. Curr. Rev. Musculoskelet. Med. *11*, 420–427.

Fears, K.P., Gonzalez-Begne, M., Love, C.T., Day, D.E., and Koo, H. (2015). Surface-induced changes in the conformation and glucan production of glucosyltransferase adsorbed on saliva-coated hydroxyapatite. Langmuir *31*, 4654–4662.

Felsburg, P.J. (2002). Overview of immune system development in the dog: comparison with humans. Hum. Exp. Toxicol. *21*, 487–492.

Flemming, H.-C., and Wingender, J. (2010). The biofilm matrix. Nat. Rev. Microbiol. *8*, 623–633.

Furustrand Tafin, U., Majic, I., Zalila Belkhodja, C., Betrisey, B., Corvec, S., Zimmerli, W., and Trampuz, A. (2011). Gentamicin improves the activities of daptomycin and vancomycin against

Enterococcus faecalis in vitro and in an experimental foreign-body infection model. Antimicrob. Agents Chemother. *55*, 4821–4827.

Furustrand Tafin, U., Corvec, S., Betrisey, B., Zimmerli, W., and Trampuz, A. (2012). Role of rifampin against Propionibacterium acnes biofilm *in vitro* and in an experimental foreign-body infection model. Antimicrob. Agents Chemother. *56*, 1885–1891.

Gibb, B.P., and Hadjiargyrou, M. (2021). Bacteriophage therapy for bone and joint infections. Bone Joint J. *103-B*, 234–244.

Gilsanz, V., Roe, T.F., Gibbens, D.T., Schulz, E.E., Carlson, M.E., Gonzalez, O., and Boechat, M.I. (1988). Effect of sex steroids on peak bone density of growing rabbits. Am. J. Physiol. *255*, E416-21.

Giulieri, S.G., Graber, P., Ochsner, P.E., and Zimmerli, W. (2004). Management of infection associated with total hip arthroplasty according to a treatment algorithm. Infection *32*, 222–228.

Godbey, T. (2016). Small Animal Handling, Care, and Anesthesia. In Handbook of Small Animal Imaging, G.C. Kagadis, N.L. Ford, D.N. Karnabatidis, and G.K. Loudos, eds. (Boca Raton (FL): CRC Press), p.

Govan, J.R., and Deretic, V. (1996). Microbial pathogenesis in cystic fibrosis: mucoid *Pseudomonas aeruginosa* and *Burkholderia cepacia*. Microbiol. Rev. *60*, 539–574.

Gristina, A.G., and Costerton, J.W. (1985). Bacterial adherence to biomaterials and tissue. The significance of its role in clinical sepsis. J. Bone Joint Surg. Am. *67*, 264–273.

Gruen, T.A., McNeice, G.M., and Amstutz, H.C. (1979). "Modes of failure" of cemented stem-type femoral components: a radiographic analysis of loosening. Clin. Orthop. Relat. Res. 17–27.

Guzmán-Soto, I., McTiernan, C., Gonzalez-Gomez, M., Ross, A., Gupta, K., Suuronen, E.J., Mah, T.-F., Griffith, M., and Alarcon, E.I. (2021). Mimicking biofilm formation and development:

Recent progress in *in vitro* and *in vivo* biofilm models. IScience *24*, 102443.

Haddad, F.S., and Bridgens, A. (2008). Infection following hip replacement: solution options. Orthopedics *31*, 907–908.

Hadden, W.J., Ibrahim, M., Taha, M., Ure, K., Liu, Y., Paish, A.D.M., Holdsworth, D.W., and Abdelbary, H. (2021). 2021 Frank Stinchfield Award: A novel cemented hip hemiarthroplasty infection model with real-time *in vivo* imaging in rats : an animal study. Bone Joint J. *103-B*, 9–16.

Hall, C.W., and Mah, T.-F. (2017). Molecular mechanisms of biofilm-based antibiotic resistance and tolerance in pathogenic bacteria. FEMS Microbiol. Rev. *41*, 276–301.

Hao, Y., Murphy, K., Lo, R.Y., Khursigara, C.M., and Lam, J.S. (2015). Single-Nucleotide Polymorphisms Found in the migA and wbpX Glycosyltransferase Genes Account for the Intrinsic Lipopolysaccharide Defects Exhibited by *Pseudomonas aeruginosa* PA14. J. Bacteriol. *197*, 2780–2791.

Hassinger, S.M., Harding, G., and Wongworawat, M.D. (2005). High-pressure pulsatile lavage propagates bacteria into soft tissue. Clin. Orthop. Relat. Res. *439*, 27–31.

Herigstad, B., Hamilton, M., and Heersink, J. (2001). How to optimize the drop plate method for enumerating bacteria. J. Microbiol. Methods *44*, 121–129.

Holsapple, M.P., West, L.J., and Landreth, K.S. (2003). Species comparison of anatomical and functional immune system development. Birth Defects Res. B. Dev. Reprod. Toxicol. *68*, 321–334.

Holstein, J.H., Garcia, P., Histing, T., Kristen, A., Scheuer, C., Menger, M.D., and Pohlemann, T. (2009). Advances in the establishment of defined mouse models for the study of fracture healing and bone regeneration. J. Orthop. Trauma *23*, S31-8.

Homma, M., DeRosier, D.J., and Macnab, R.M. (1990). Flagellar hook and hook-associated proteins of *Salmonella typhimurium* and their relationship to other axial components of the flagellum. J. Mol. Biol. *213*, 819–832.

Hsieh, P.-H., Lee, M.S., Hsu, K.-Y., Chang, Y.-H., Shih, H.-N., and Ueng, S.W. (2009). Gram-negative prosthetic joint infections: risk factors and outcome of treatment. Clin. Infect. Dis. an Off. Publ. Infect. Dis. Soc. Am. *49*, 1036–1043.

Jamei, O., Gjoni, S., Zenelaj, B., Kressmann, B., Belaieff, W., Hannouche, D., and Uckay, I. (2017). Which Orthopaedic Patients Are Infected with Gram-negative Non-fermenting Rods? J. Bone Jt. Infect. *2*, 73–76.

Jämsen, E., Huhtala, H., Puolakka, T., and Moilanen, T. (2009). Risk factors for infection after knee arthroplasty. A register-based analysis of 43,149 cases. J. Bone Joint Surg. Am. *91*, 38–47.

Jeys, L.M., Grimer, R.J., Carter, S.R., and Tillman, R.M. (2005). Periprosthetic infection in patients treated for an orthopaedic oncological condition. J. Bone Joint Surg. Am. *87*, 842–849.

John, A.-K., Baldoni, D., Haschke, M., Rentsch, K., Schaerli, P., Zimmerli, W., and Trampuz, A. (2009). Efficacy of daptomycin in implant-associated infection due to methicillin-resistant *Staphylococcus aureus*: importance of combination with rifampin. Antimicrob. Agents Chemother. *53*, 2719–2724.

Kalbian, I.L., Goswami, K., Tan, T.L., John, N., Foltz, C., Parvizi, J., and Arnold, W. V (2020). Treatment Outcomes and Attrition in Gram-Negative Periprosthetic Joint Infection. J. Arthroplasty *35*, 849–854.

Kamath, A.F., Ong, K.L., Lau, E., Chan, V., Vail, T.P., Rubash, H.E., Berry, D.J., and Bozic, K.J. (2015). Quantifying the Burden of Revision Total Joint Arthroplasty for Periprosthetic Infection. J. Arthroplasty *30*, 1492–1497.

Kessler, B., Sendi, P., Graber, P., Knupp, M., Zwicky, L., Hintermann, B., and Zimmerli, W. (2012). Risk factors for periprosthetic ankle joint infection: a case-control study. J. Bone Joint Surg. Am. *94*, 1871–1876.

Kimmel, D.B., and Jee, W.S. (1982). A quantitative histologic study of bone turnover in young adult beagles. Anat. Rec. *203*, 31–45.

Kunutsor, S.K., Whitehouse, M.R., Blom, A.W., Board, T., Kay, P., Wroblewski, B.M., Zeller, V., Chen, S.-Y., Hsieh, P.-H., Masri, B.A., et al. (2018). One- and two-stage surgical revision of peri-prosthetic joint infection of the hip: a pooled individual participant data analysis of 44 cohort studies. Eur. J. Epidemiol. *33*, 933–946.

Kurtz, S.M., Lau, E.C., Son, M.-S., Chang, E.T., Zimmerli, W., and Parvizi, J. (2018). Are We Winning or Losing the Battle With Periprosthetic Joint Infection: Trends in Periprosthetic Joint Infection and Mortality Risk for the Medicare Population. J. Arthroplasty *33*, 3238–3245.

Laffer, R.R., Graber, P., Ochsner, P.E., and Zimmerli, W. (2006). Outcome of prosthetic knee-associated infection: evaluation of 40 consecutive episodes at a single centre. Clin. Microbiol. Infect. Off. Publ. Eur. Soc. Clin. Microbiol. Infect. Dis. *12*, 433–439.

Lazurko, C., Khatoon, Z., Goel, K., Sedlakova, V., Eren Cimenci, C., Ahumada, M., Zhang, L., Mah, T.-F., Franco, W., Suuronen, E.J., et al. (2020). Multifunctional Nano and Collagen-Based Therapeutic Materials for Skin Repair. ACS Biomater. Sci. Eng. *6*, 1124–1134.

Lenguerrand, E., Whitehouse, M.R., Beswick, A.D., Kunutsor, S.K., Burston, B., Porter, M., and Blom, A.W. (2018). Risk factors associated with revision for prosthetic joint infection after hip replacement: a prospective observational cohort study. Lancet. Infect. Dis. *18*, 1004–1014.

Letamendia, A., Quevedo, C., Ibarbia, I., Virto, J.M., Holgado, O., Diez, M., Izpisua Belmonte, J.C., and Callol-Massot, C. (2012). Development and validation of an automated high-throughput

system for zebrafish *in vivo* screenings. PLoS One *7*, e36690.

Li, C., Renz, N., and Trampuz, A. (2018). Management of Periprosthetic Joint Infection. Hip Pelvis *30*, 138–146.

Li, C., Renz, N., Trampuz, A., and Ojeda-Thies, C. (2020). Twenty common errors in the diagnosis and treatment of periprosthetic joint infection. Int. Orthop. *44*, 3–14.

Li, D., Gromov, K., Søballe, K., Puzas, J.E., O'Keefe, R.J., Awad, H., Drissi, H., and Schwarz, E.M. (2008). Quantitative mouse model of implant-associated osteomyelitis and the kinetics of microbial growth, osteolysis, and humoral immunity. J. Orthop. Res. Off. Publ. Orthop. Res. Soc. *26*, 96–105.

Li, G., Guo, F., Ou, Y., Dong, G., and Zhou, W. (2013). Epidemiology and outcomes of surgical site infections following orthopedic surgery. Am. J. Infect. Control *41*, 1268–1271.

Liu, Y., and Tay, J.H. (2001). Metabolic response of biofilm to shear stress in fixed-film culture. J. Appl. Microbiol. *90*, 337–342.

López, D., Vlamakis, H., and Kolter, R. (2010). Biofilms. Cold Spring Harb. Perspect. Biol. *2*, a000398.

Lovati, A.B., Bottagisio, M., de Vecchi, E., Gallazzi, E., and Drago, L. (2017). Animal Models of Implant-Related Low-Grade Infections. A Twenty-Year Review. Adv. Exp. Med. Biol. *971*, 29–50.

Mack, D., Fischer, W., Krokotsch, A., Leopold, K., Hartmann, R., Egge, H., and Laufs, R. (1996). The intercellular adhesin involved in biofilm accumulation of *Staphylococcus epidermidis* is a linear beta-1,6-linked glucosaminoglycan: purification and structural analysis. J. Bacteriol. *178*, 175–183.

Mah, T.F., and O'Toole, G.A. (2001). Mechanisms of biofilm resistance to antimicrobial agents.

Trends Microbiol. *9*, 34–39.

Marschall, J., Lane, M.A., Beekmann, S.E., Polgreen, P.M., and Babcock, H.M. (2013). Current management of prosthetic joint infections in adults: results of an Emerging Infections Network survey. Int. J. Antimicrob. Agents *41*, 272–277.

Martiniaková, M., Omelka, R., Chrenek, P., Ryban, L., Parkányi, V., Grosskopf, B., Vondráková, M., and Bauerová, M. (2005). Changes of femoral bone tissue microstructure in transgenic rabbits. Folia Biol. (Praha). *51*, 140–144.

Matar, W.Y., Jafari, S.M., Restrepo, C., Austin, M., Purtill, J.J., and Parvizi, J. (2010). Preventing infection in total joint arthroplasty. J. Bone Joint Surg. Am. *92 Suppl 2*, 36–46.

Merritt, J.H., Kadouri, D.E., and O'Toole, G.A. (2005). Growing and analyzing static biofilms. Curr. Protoc. Microbiol. *Chapter 1*, Unit 1B.1.

Mikkelsen, H., McMullan, R., and Filloux, A. (2011). The *Pseudomonas aeruginosa* reference strain PA14 displays increased virulence due to a mutation in ladS. PLoS One *6*, e29113.

Millhouse, E., Jose, A., Sherry, L., Lappin, D.F., Patel, N., Middleton, A.M., Pratten, J., Culshaw, S., and Ramage, G. (2014). Development of an *in vitro* periodontal biofilm model for assessing antimicrobial and host modulatory effects of bioactive molecules. BMC Oral Health *14*, 80.

Mills, A.L., Powelson, D.K., and Fletcher, M. (1996). Bacterial adhesion: molecular and ecological diversity. Surf. Sci. Rep. *37*, 25–40.

Moradali, M.F., Ghods, S., and Rehm, B.H.A. (2017). *Pseudomonas aeruginosa* Lifestyle: A Paradigm for Adaptation, Survival, and Persistence. Front. Cell. Infect. Microbiol. *7*, 39.

Moran, E., Masters, S., Berendt, A.R., McLardy-Smith, P., Byren, I., and Atkins, B.L. (2007). Guiding empirical antibiotic therapy in orthopaedics: The microbiology of prosthetic joint infection managed by debridement, irrigation and prosthesis retention. J. Infect. *55*, 1–7.

Muñoz-Mahamud, E., García, S., Bori, G., Martínez-Pastor, J.C., Zumbado, J.A., Riba, J., Mensa, J., and Soriano, A. (2011). Comparison of a low-pressure and a high-pressure pulsatile lavage during débridement for orthopaedic implant infection. Arch. Orthop. Trauma Surg. *131*, 1233–1238.

Neely, M.N., Pfeifer, J.D., and Caparon, M. (2002). Streptococcus-zebrafish model of bacterial pathogenesis. Infect. Immun. *70*, 3904–3914.

Newman, E., Turner, A.S., and Wark, J.D. (1995). The potential of sheep for the study of osteopenia: current status and comparison with other animal models. Bone *16*, 277S-284S.

Nickel, J.C., Ruseska, I., Wright, J.B., and Costerton, J.W. (1985). Tobramycin resistance of *Pseudomonas aeruginosa* cells growing as a biofilm on urinary catheter material. Antimicrob. Agents Chemother. *27*, 619–624.

Nijhof, M.W., Dhert, W.J., Fleer, A., Vogely, H.C., and Verbout, A.J. (2000). Prophylaxis of implant-related *staphylococcal* infections using tobramycin-containing bone cement. J. Biomed. Mater. Res. *52*, 754–761.

Nishitani, K., Sutipornpalangkul, W., de Mesy Bentley, K.L., Varrone, J.J., Bello-Irizarry, S.N., Ito, H., Matsuda, S., Kates, S.L., Daiss, J.L., and Schwarz, E.M. (2015). Quantifying the natural history of biofilm formation *in vivo* during the establishment of chronic implant-associated *Staphylococcus aureus* osteomyelitis in mice to identify critical pathogen and host factors. J. Orthop. Res. Off. Publ. Orthop. Res. Soc. *33*, 1311–1319.

Niska, J.A., Meganck, J.A., Pribaz, J.R., Shahbazian, J.H., Lim, E., Zhang, N., Rice, B.W., Akin, A., Ramos, R.I., Bernthal, N.M., et al. (2012). Monitoring bacterial burden, inflammation and bone damage longitudinally using optical and μCT imaging in an orthopaedic implant infection in mice. PLoS One *7*, e47397.

Nowatzki, P.J., Koepsel, R.R., Stoodley, P., Min, K., Harper, A., Murata, H., Donfack, J., Hortelano, E.R., Ehrlich, G.D., and Russell, A.J. (2012). Salicylic acid-releasing polyurethane acrylate polymers as anti-biofilm urological catheter coatings. Acta Biomater. *8*, 1869–1880.

Nunamaker, D.M. (1998). Experimental models of fracture repair. Clin. Orthop. Relat. Res. S56-65.

O'Toole, G.A., and Kolter, R. (1998). Flagellar and twitching motility are necessary for *Pseudomonas aeruginosa* biofilm development. Mol. Microbiol. *30*, 295–304.

O'Toole, G., Kaplan, H.B., and Kolter, R. (2000). Biofilm Formation as Microbial Development. Annu. Rev. Microbiol. *54*, 49–79.

Olsen, I. (2015). Biofilm-specific antibiotic tolerance and resistance. Eur. J. Clin. Microbiol. Infect. Dis. Off. Publ. Eur. Soc. Clin. Microbiol. *34*, 877–886.

Otto, M. (2008). *Staphylococcal* biofilms. Curr. Top. Microbiol. Immunol. *322*, 207–228.

Paish, A.D.M., Nikolov, H.N., El-Warrak, A.O., Welch, I., Teeter, M.G., Naudie, D.D., and Holdsworth, D.W. Towards optimizing a custom small animal model of partial joint replacement system created via additive manufacturing. Front. Bioeng. Biotechnol.

Paish, A.D.M., Nikolov, H.N., Welch, I.D., El-Warrak, A.O., Teeter, M.G., Naudie, D.D.R., and Holdsworth, D.W. (2020). Image-based design and 3D-metal printing of a rat hip implant for use in a clinically representative model of joint replacement. J. Orthop. Res. Off. Publ. Orthop. Res. Soc. *38*, 1627–1636.

Parvizi, J., Tan, T.L., Goswami, K., Higuera, C., Della Valle, C., Chen, A.F., and Shohat, N. (2018). The 2018 Definition of Periprosthetic Hip and Knee Infection: An Evidence-Based and Validated Criteria. J. Arthroplasty *33*, 1309-1314.e2.

Peel, T.N., Cheng, A.C., Buising, K.L., and Choong, P.F.M. (2012). Microbiological aetiology,

epidemiology, and clinical profile of prosthetic joint infections: are current antibiotic prophylaxis guidelines effective? Antimicrob. Agents Chemother. *56*, 2386–2391.

Petty, W., Spanier, S., Shuster, J.J., and Silverthorne, C. (1985). The influence of skeletal implants on incidence of infection. Experiments in a canine model. J. Bone Joint Surg. Am. *67*, 1236–1244.

Petty, W., Spanier, S., and Shuster, J.J. (1988). Prevention of infection after total joint replacement. Experiments with a canine model. J. Bone Joint Surg. Am. *70*, 536–539.

Poultsides, L.A., Papatheodorou, L.K., Karachalios, T.S., Khaldi, L., Maniatis, A., Petinaki, E., and Malizos, K.N. (2008). Novel model for studying hematogenous infection in an experimental setting of implant-related infection by a community-acquired methicillin-resistant S. aureus strain. J. Orthop. Res. Off. Publ. Orthop. Res. Soc. *26*, 1355–1362.

Powers, D.L., Claassen, B., and Black, J. (1995). The rat as an animal model for total hip replacement arthroplasty. J. Investig. Surg. Off. J. Acad. Surg. Res. *8*, 349–362.

Del Pozo, J.L., and Patel, R. (2009). Infection Associated with Prosthetic Joints. N. Engl. J. Med. *361*, 787–794.

Premkumar, A., Kolin, D.A., Farley, K.X., Wilson, J.M., McLawhorn, A.S., Cross, M.B., and Sculco, P.K. (2021a). Projected Economic Burden of Periprosthetic Joint Infection of the Hip and Knee in the United States. J. Arthroplasty *36*, 1484-1489.e3.

Premkumar, A., Nishtala, S.N., Nguyen, J.T., Bostrom, M.P.G., and Carli, A. V (2021b). The AAHKS Best Podium Presentation Research Award: Comparing the Efficacy of Irrigation Solutions on *Staphylococcal* Biofilm Formed on Arthroplasty Surfaces. J. Arthroplasty *36*, S26–S32.

Pribaz, J.R., Bernthal, N.M., Billi, F., Cho, J.S., Ramos, R.I., Guo, Y., Cheung, A.L., Francis, K.P., and Miller, L.S. (2012). Mouse model of chronic post-arthroplasty infection: noninvasive *in vivo*

bioluminescence imaging to monitor bacterial burden for long-term study. J. Orthop. Res. *30*, 335–340.

Pulido, L., Ghanem, E., Joshi, A., Purtill, J.J., and Parvizi, J. (2008). Periprosthetic joint infection: the incidence, timing, and predisposing factors. Clin. Orthop. Relat. Res. *466*, 1710–1715.

Ramachandran, G. (2014). Gram-positive and gram-negative bacterial toxins in sepsis: a brief review. Virulence *5*, 213–218.

Reizner, W., Hunter, J.G., O'Malley, N.T., Southgate, R.D., Schwarz, E.M., and Kates, S.L. (2014). A systematic review of animal models for *Staphylococcus aureus* osteomyelitis. Eur. Cell. Mater. *27*, 196–212.

Ribera, A., Benavent, E., Lora-Tamayo, J., Tubau, F., Pedrero, S., Cabo, X., Ariza, J., and Murillo, O. (2015). Osteoarticular infection caused by MDR *Pseudomonas aeruginosa*: the benefits of combination therapy with colistin plus β-lactams. J. Antimicrob. Chemother. *70*, 3357–3365.

Rodríguez-Pardo, D., Pigrau, C., Lora-Tamayo, J., Soriano, A., del Toro, M.D., Cobo, J., Palomino, J., Euba, G., Riera, M., Sánchez-Somolinos, M., et al. (2014). Gram-negative prosthetic joint infection: outcome of a debridement, antibiotics and implant retention approach. A large multicentre study. Clin. Microbiol. Infect. Off. Publ. Eur. Soc. Clin. Microbiol. Infect. Dis. *20*, O911-9.

Romero-Calle, D., Guimarães Benevides, R., Góes-Neto, A., and Billington, C. (2019). Bacteriophages as Alternatives to Antibiotics in Clinical Care. Antibiot. *8*.

Rosenthal, V.D., Al-Abdely, H.M., El-Kholy, A.A., AlKhawaja, S.A.A., Leblebicioglu, H., Mehta, Y., Rai, V., Hung, N.V., Kanj, S.S., Salama, M.F., et al. (2016). International Nosocomial Infection Control Consortium report, data summary of 50 countries for 2010-2015: Device-associated module. Am. J. Infect. Control *44*, 1495–1504.

Russell, M.A., and Darzins, A. (1994). The *pilE* gene product of *Pseudomonas aeruginosa*, required for pilus biogenesis, shares amino acid sequence identity with the N-termini of type 4 prepilin proteins. Mol. Microbiol. *13*, 973–985.

van Schaik, E.J., Giltner, C.L., Audette, G.F., Keizer, D.W., Bautista, D.L., Slupsky, C.M., Sykes, B.D., and Irvin, R.T. (2005). DNA binding: a novel function of *Pseudomonas aeruginosa* type IV pili. J. Bacteriol. *187*, 1455–1464.

Schwank, S., Rajacic, Z., Zimmerli, W., and Blaser, J. (1998). Impact of bacterial biofilm formation on *in vitro* and *in vivo* activities of antibiotics. Antimicrob. Agents Chemother. *42*, 895–898.

Sendi, P., and Zimmerli, W. (2012). Antimicrobial treatment concepts for orthopaedic device-related infection. Clin. Microbiol. Infect. Off. Publ. Eur. Soc. Clin. Microbiol. Infect. Dis. *18*, 1176–1184.

Shah, N.B., Osmon, D.R., Steckelberg, J.M., Sierra, R.J., Walker, R.C., Tande, A.J., and Berbari, E.F. (2016). *Pseudomonas* Prosthetic Joint Infections: A Review of 102 Episodes. J. Bone Jt. Infect. *1*, 25–30.

Simpson, D.A., Ramphal, R., and Lory, S. (1995). Characterization of *Pseudomonas aeruginosa fliO*, a gene involved in flagellar biosynthesis and adherence. Infect. Immun. *63*, 2950–2957.

Skovbjerg, S., Martner, A., Hynsjö, L., Hessle, C., Olsen, I., Dewhirst, F.E., Tham, W., and Wold, A.E. (2010). Gram-positive and gram-negative bacteria induce different patterns of cytokine production in human mononuclear cells irrespective of taxonomic relatedness. J. Interf. Cytokine Res. Off. J. Int. Soc. Interf. Cytokine Res. *30*, 23–32.

Stocks, G.W., O'Connor, D.P., Self, S.D., Marcek, G.A., and Thompson, B.L. (2011). Directed air flow to reduce airborne particulate and bacterial contamination in the surgical field during total

hip arthroplasty. J. Arthroplasty *26*, 771–776.

Stoodley, P., Ehrlich, G.D., Sedghizadeh, P.P., Hall-Stoodley, L., Baratz, M.E., Altman, D.T., Sotereanos, N.G., Costerton, J.W., and Demeo, P. (2011). Orthopaedic biofilm infections. Curr. Orthop. Pract. *22*, 558–563.

Sun, Y., Dowd, S.E., Smith, E., Rhoads, D.D., and Wolcott, R.D. (2008). *In vitro* multispecies Lubbock chronic wound biofilm model. Wound Repair Regen. Off. Publ. Wound Heal. Soc. [and] Eur. Tissue Repair Soc. *16*, 805–813.

Thompson, J.M., Miller, R.J., Ashbaugh, A.G., Dillen, C.A., Pickett, J.E., Wang, Y., Ortines, R. V, Sterling, R.S., Francis, K.P., Bernthal, N.M., et al. (2018). Mouse model of Gram-negative prosthetic joint infection reveals therapeutic targets. JCI Insight *3*.

Trampuz, A., Murphy, C.K., Rothstein, D.M., Widmer, A.F., Landmann, R., and Zimmerli, W. (2007). Efficacy of a novel rifamycin derivative, ABI-0043, against *Staphylococcus aureus* in an experimental model of foreign-body infection. Antimicrob. Agents Chemother. *51*, 2540–2545.

Tsukayama, D.T., Estrada, R., and Gustilo, R.B. (1996). Infection after total hip arthroplasty. A study of the treatment of one hundred and six infections. J. Bone Joint Surg. Am. *78*, 512–523.

Tzeng, A., Tzeng, T.H., Vasdev, S., Korth, K., Healey, T., Parvizi, J., and Saleh, K.J. (2015). Treating periprosthetic joint infections as biofilms: key diagnosis and management strategies. Diagn. Microbiol. Infect. Dis. *81*, 192–200.

Urish, K.L., DeMuth, P.W., Craft, D.W., Haider, H., and Davis, C.M. 3rd (2014). Pulse lavage is inadequate at removal of biofilm from the surface of total knee arthroplasty materials. J. Arthroplasty *29*, 1128–1132.

Urish, K.L., Bullock, A.G., Kreger, A.M., Shah, N.B., Jeong, K., and Rothenberger, S.D. (2018). A Multicenter Study of Irrigation and Debridement in Total Knee Arthroplasty Periprosthetic Joint

Infection: Treatment Failure Is High. J. Arthroplasty *33*, 1154–1159.

Vielgut, I., Sadoghi, P., Wolf, M., Holzer, L., Leithner, A., Schwantzer, G., Poolman, R., Frankl, B., and Glehr, M. (2015). Two-stage revision of prosthetic hip joint infections using antibiotic-loaded cement spacers: When is the best time to perform the second stage? Int. Orthop. *39*, 1731–1736.

Vincze, T., Posfai, J., and Roberts, R.J. (2003). NEBcutter: A program to cleave DNA with restriction enzymes. Nucleic Acids Res. *31*, 3688–3691.

Wang, X., Mabrey, J.D., and Agrawal, C.M. (1998). An interspecies comparison of bone fracture properties. Biomed. Mater. Eng. *8*, 1–9.

Widmer, A.F., Colombo, V.E., Gächter, A., Thiel, G., and Zimmerli, W. (1990). *Salmonella* infection in total hip replacement: tests to predict the outcome of antimicrobial therapy. Scand. J. Infect. Dis. *22*, 611–618.

Wijeyekoon, S., Mino, T., Satoh, H., and Matsuo, T. (2004). Effects of substrate loading rate on biofilm structure. Water Res. *38*, 2479–2488.

Wolfgang, M.C., Jyot, J., Goodman, A.L., Ramphal, R., and Lory, S. (2004). *Pseudomonas aeruginosa* regulates flagellin expression as part of a global response to airway fluid from cystic fibrosis patients. Proc. Natl. Acad. Sci. U. S. A. *101*, 6664–6668.

Xu, C., Goswami, K., Li, W.T., Tan, T.L., Yayac, M., Wang, S.-H., and Parvizi, J. (2020). Is Treatment of Periprosthetic Joint Infection Improving Over Time? J. Arthroplasty *35*, 1696-1702.e1.

Yang, X., Ricciardi, B.F., Dvorzhinskiy, A., Brial, C., Lane, Z., Bhimani, S., Burket, J.C., Hu, B., Sarkisian, A.M., Ross, F.P., et al. (2015). Intermittent Parathyroid Hormone Enhances Cancellous Osseointegration of a Novel Murine Tibial Implant. J. Bone Joint Surg. Am. *97*, 1074–1083.

Ziegler, A., Gonzalez, L., and Blikslager, A. (2016). Large Animal Models: The Key to Translational Discovery in Digestive Disease Research. Cell. Mol. Gastroenterol. Hepatol. *2*, 716–724.

Zimmerli, W. (2014). Clinical presentation and treatment of orthopaedic implant-associated infection. J. Intern. Med. *276*, 111–119.

Zimmerli, W., and Moser, C. (2012). Pathogenesis and treatment concepts of orthopaedic biofilm infections. FEMS Immunol. Med. Microbiol. *65*, 158–168.

Zimmerli, W., Widmer, A.F., Blatter, M., Frei, R., and Ochsner, P.E. (1998). Role of rifampin for treatment of orthopedic implant-related *staphylococcal* infections: a randomized controlled trial. Foreign-Body Infection (FBI) Study Group. JAMA *279*, 1537–1541.

Zimmerli, W., Trampuz, A., and Ochsner, P.E. (2004). Prosthetic-joint infections. N. Engl. J. Med. *351*, 1645–1654.

Zmistowski, B., Fedorka, C.J., Sheehan, E., Deirmengian, G., Austin, M.S., and Parvizi, J. (2011). Prosthetic joint infection caused by gram-negative organisms. J. Arthroplasty *26*, 104–108.

CONTRIBUTION OF COLLABORATORS:

- **Clayton Hall** Construction of bioluminescent PA14 strain (PA14-*lux*)
- **Li Zhang** and **Caetanie Tchagang**, for all their help with the technical aspects of experiments that were completed in the lab.
- **Dr. Adam Paish** (and the **David Wayne Holdsworth Lab**, the University of Western Ontario), for their help with everything related to the creation of 3D printed medical grade titanium hip implants.
- **Dr. Kerstin Ure** and the animal behavior, physiology core, University of Ottawa, Faculty of Medicine, Ottawa, Canada, for their help in digiGait analysis.
- **Yun Liu** and the materials characterization core facility, centre for advanced materials research (camar), University of Ottawa, Ottawa, Canada for her help in scanning electron microscopy

CURRICULUM VITAE

Mazen M Ibrahim MBBCh MSc MD PhD • Contact: The Ottawa Hospital 501 Smyth Road, Ottawa, Ontario K1H8L6, Canada	• Position: Orthopaedic Surgeon Assistant Professor https://uniweb.uottawa.ca/members/4483/profile

Education/Training:

2020-2021 University of Ottawa
Master's in Microbiology and Immunology Specialization in Pathology and Experimental Medicine

2019 Children Hospital Eastern Ontario (CHEO)
Clinical Fellowship Pediatric Orthopedic

2017-2018 University of Ottawa/The Ottawa Hospital (TOH)
Clinical Fellowship Arthroplasty and Adult Reconstruction

2015-2016 Children Hospital of Philadelphia (CHOP) Philadelphia, PA, United States
Research Fellowship Pediatric Orthopedic and Translational Medicine Research

2016 Saint Marry Hospital, Paly`s institute/ West Palm beach, Florida, United States
Travelling Fellowship Deformity and Limb lengthening

2015 National University Hospital of Singapore (NUHS), Singapore
Clinical Fellowship Pediatric Orthopedic

2012 Heidelberg Örthopadie/Heidelberg University, Heidelberg, Germany
Foot and ankle surgery

2011 InselSpital, Bern University Hospital, Switzerland
Clinical AO Fellowship Pelvis trauma and hip reconstruction

Faculty of Medicine, Mansoura University, Egypt
2015 Doctorate (MD/PhD) Orthopaedic Surgery
2007 Master (MSc) Orthopaedic Surgery
2002 Bachelor of medicine and surgery MBBCh

Current Employment

2020 August: **Assistant Professor**, Department of Surgery/Orthopaedic, University of Ottawa.
2022 January: **Clinician Investigator** in the Clinical Epidemiology Program (CEP) at the Ottawa Hospital Research Institute (OHRI)

Past Professional Experiences and Independent Practice:

October 2018-January 2019: **Saudi German Hospital, Cairo, Egypt**. Consultant Orthopaedics
May 2009-Feb 2015: **Al Razi hospital, Minister of health, Kuwait.** Registrar Orthopaedics
Feb 2008-May 2009: **Dar Al Fouad Hospital, Cairo, Egypt**, Registrar Orthopaedics
May 2004-Oct 2004: **Ministry of Health, Dakahlia health district, Egypt,** General practitioner physician.

Grants and Research Awards

2021 Frank Stinchfield Award, The Hip Society
Project: A novel cemented hip hemiarthroplasty infection model with real-time *in vivo* imaging in rats

2020 Hans K. Uhthoff, MD FRCSC Graduate Fellowship (712240301930), uOttawa
Amount: 15,000 CAD
Program: Master of Science Microbiology and Immunology Specialization in Pathology and Experimental Medicine
Supervisors: Thien-Fah Mah PhD (Graduate supervisor)
Project: Developing Periprosthetic Joint Infection Animal Model testing novel therapeutics and Biofilm formation

2016 Children Hospital of Philadelphia CHOP (Internal Grant)
Amount: 13,500 USD
Role: Co-investigator
PIs: J. Todd Lawrence (CHOP), Leo Han (Drexel University) and Mauricio Pacifici (CHOP)
Project: Novel Microfiber Scaffold for Cartilage Repair

2015 SICOT/CHOP fellowship by La Société Internationale de Chirurgie Orthopédique et de Traumatologie (SICOT)
Amount: 40,000 USD
Supervisor: Mauricio Pacifici (CHOP)
Project: Translational Medicine Research Use of Mouse Model in Hereditary Multiple Exostosis Hip Development and Pediatric Orthopedic Clinical Research.

2011 AO Foundation/AO Trauma Fellowship
Amount: 3,000 CHf
Supervisor: Prof.Dr.med. Klaus Siebenrock (InselSpital)
Hip preservation surgery and hip reconstruction

Affiliations and Memberships:

National:
Medical Council of Canada (MCC) since July 2016 (valid)
Canadian Orthopaedic Association (COA) since July 2016 (valid)
College of Physicians and Surgeons of Ontario (CPSO) Postgraduate education (Clinical Fellow) since Mar 2017

International:
Egyptian Medical Syndicate (EMS): Consultant of Orthopedic Surgery, since May 2015 (valid)
Penn Center for Musculoskeletal Disorders (Associate Member) since November 2015 (valid)
LLRS (Limb Lengthening and Reconstruction society) since July 2014 (valid)
Egyptian Orthopedic Association (EOA) since October 2004 (valid)

Past affiliations:
Kuwait Medical Association (KMA): Specialist registrar of Orthopedic Surgery, June 2009-February 2015
Singaporean Medical Council (SMC): Temporary registration (Clinical Fellow) April 2015- August 2015

Medical Equivalence Certification:

Medical Council of Canada Evaluating Examination (MCCEE) MCC candidate #: 1490861877
United States Medical License Examination (USMLE/ECFMG #: 0-900-858-2).

Invited Reviewer:

Journal of Arthroplasty (January 2021-now)
The Foot Journal (November 2020-now)
Journal of Knee Surgery (November 2018-now)
World Journal of Orthopaedics (January 2015-2018)

Book Chapters:

Ibrahim MM, Smit K (2020) Anatomical Description and Classification of Hip Dysplasia. In: Beaulé P. (eds) Hip Dysplasia. Springer, Cham

Ibrahim MM, Beaule PE (under edition) Open Surgical Dislocation Approach Positioning and Operative Set-Up. In: Allston Stubbs A. (eds) Hip Surgery: Tricks of the Trade. (under-edition)

Peer-Reviewed Publications:

Ibrahim MM; Liu Y; Ure K; Hall CW; Mah TF; Abdelbary H, Establishment of a Novel Gram-Negative Prosthetic Joint Infection Rat Model Using Uncemented Hip Hemiarthroplasty (Submitted to the Journal of Bone and Joint (JBJS), January 2022)

Ibrahim MM, Smit K, Poitras S, Grammatopoulos G, Beaulé PE. Correlation of Patient-Reported Outcomes After Periacetabular Osteotomy with Femoral Head Coverage and Acetabular Orientation: A Single-Center Cohort Study. Am J Sports Med. 2021 Apr;49(5):1209-1219.

Hadden WJ, **Ibrahim M**, Taha M, Ure K, Liu Y, Paish ADM, Holdsworth DW, Abdelbary H. 2021 Frank Stinchfield Award: A novel cemented hip hemiarthroplasty infection model with real-time *in vivo* imaging in rats: an animal study. Bone Joint J. 2021 Jul;103-B(7 Supple B):9-16.

Gofton WT, **Ibrahim MM**, Kreviazuk CJ, Kim PR, Feibel RJ, Beaulé PE. Ten-Year Experience with the Anterior Approach to Total Hip Arthroplasty at a Tertiary Care Center. J Arthroplasty. 2020 May;35(5):1281-1289.e1.

Bali K, Smit K, **Ibrahim MM**, Poitras S, Wilkin G, Galmiche R, Belzile E, Beaulé PE. Ottawa classification for symptomatic acetabular dysplasia assessment of interobserver and intraobserver reliability. Bone & Joint Research. 2020 May;9(5):242-9.

Al-Mahdi W, **Ibrahim MM**, Spiegel DA, Arkader A, Nance M, Baldwin K. Is Systemic Inflammatory Response Syndrome Relevant to Pulmonary Complications and Mortality in Multiply Injured Children? J Pediatr Orthop. 2020 Jan;40(1):1-7.

Ibrahim MM, El-Lakkany MR, Wahba MM, El-Ganainy AA, Aly AM. Combined open reduction and Dega transiliac osteotomy for developmental dysplasia of the hip in walking children. Acta Orthop Belg. 2019;85(4):545-553.

Wang M, Cui C, **Ibrahim MM**, Han B, Li Q, Pacifici M, Lawrence JTR, Han L, Han LH, Regulating Mechanotransduction in Three Dimensions using Sub-Cellular Scale, Crosslinkable Fibers of Controlled Diameter, Stiffness, and Alignment. Adv. Funct. Mater. 2019, 29, 1808967.

Ibrahim MM, Poitras S, Bunting AC, Sandoval E, Beaulé PE. Does acetabular coverage influence the clinical outcome of arthroscopically treated cam-type femoroacetabular impingement (FAI)? Bone Joint J. 2018 Jul;100-B(7):831-838.

Tan SHS, **Ibrahim MM**, Lee ZJ, Chee YKM, Hui JH. Patellar tracking should be taken into account when measuring radiographic parameters for recurrent patellar instability. Knee Surg Sports Traumatol Arthrosc. 2018 Dec;26(12):3593-3600.

Wilkin GP, **Ibrahim MM**, Smit KM, Beaulé PE. A Contemporary Definition of Hip Dysplasia and Structural Instability: Toward a Comprehensive Classification for Acetabular Dysplasia. J Arthroplasty. 2017;32(9S):S20-S27.

Sinha S, Mundy C, Bechtold T, Sgariglia F, **Ibrahim MM**, Billings PC, Carroll K, Koyama E, Jones KB, Pacifici M. Unsuspected osteochondroma-like outgrowths in the cranial base of Hereditary Multiple Exostoses patients and modeling and treatment with a BMP antagonist in mice. PLoS Genet. 2017 Apr 26;13(4):e1006742.

Abou Elatta MM, Assal F, Basheer HM, **Ibrahim MM**. The Use of a Simple Dynamic External Fixator for the Treatment of Volar Fracture Subluxation of Proximal Interphalangeal Joints of the Fingers. Tech Hand Up Extrem Surg. 2016;20(4):161-165.

Ibrahim MM "Dega Transiliac Osteotomy in Developmental Dysplasia of the Hip". A thesis submitted to Mansoura University for the MD/PhD Degree in Orthopedic Surgery (2015)

Kishta WE, Mansour EH, **Ibrahim MM**. The accessory soleus muscle as a cause of persistent equinus in clubfeet treated by the Ponseti method: A report of 16 cases. Acta Orthop Belg. 2010;76(5):658-662.

Elshenawy EM, Hassanen EY, Ramadam AI, **Ibrahim MM**. The Mansoura experience in the treatment of idiopathic clubfoot deformity using the Ponseti technique. Acta Orthop Belg. 2008;74(5):659-666.

Ibrahim MM "Short Term Results of Ponseti Technique in Treatment of Idiopathic Congenital Talipes Equinovarus". A thesis submitted to Mansoura University for the Master-Degree in Orthopedic Surgery (2007)

Oral Presentations and Posters:

ORS (Orthopaedic Research Society Annual meeting) Tampa, Florida, February 2022, Poster presentation "Establishment of Biofilm-Based Prosthetic Joint Infection Rat Model"

AAOS (American Academy of Orthopaedic Surgeons Annual meeting) San-Diego, CA, August 2021 Oral presentation: "How do Patient Reported Outcomes Correlate to Acetabular Coverage After Periacetabular Osteotomy?"

AAOS (American Academy of Orthopaedic Surgeons Annual meeting) San-Diego, CA, August 2021 Poster presentation: "A novel cemented hip hemiarthroplasty infection model with real-time *in vivo* imaging in rats"

COA (Canadian Orthopaedic Association Annual meeting) June 2021 Virtual Oral presentation “Correlation of Patient-Reported Outcomes After Periacetabular Osteotomy with Femoral Head Coverage and Acetabular Orientation”

CSM-SCM (Canadian Society of Microbiologist Annual Conference) Remote June 2021 Early Career Researcher Section Symposia, Oral Presentation “Establishment of Prosthetic Joint Infection Rat Model”

ORS (Orthopedic Research Society) Annual meeting, Phoenix, February 2020 Oral presentation: **“**How do Patient Reported Outcomes Correlate to Acetabular Coverage After Periacetabular Osteotomy?”

ORS (Orthopedic Research Society) annual meeting, New Orleans, March 2018, Louisiana. Poster presentation: “Does Acetabular Coverage Influence the Clinical Outcome of Arthroscopically Treated Cam Femoroacetabular Impingement”.

AAOS (American Academy of Orthopaedic Surgeons) annual meeting New Orleans, March 2018. Louisiana: Event Type: Symposium Faculty: “Everything You Need to Know About Simple and Complex Primary Total Hip Arthroplasty”.

EFORT 19th Congress Barcelona, May 2018, Spain. Poster presentation: “Safety and Effectiveness Of DAA-THA: A Decade`s Experience at a Tertiary Care Center”.

COA (Canadian Orthopedic association) annual meeting, Victoria BC, June 2018, Canada. Oral Presentation: “Does Acetabular Coverage Influence the Clinical Outcome of Arthroscopically Treated Cam Femoroacetabular Impingement”.

COA (Canadian Orthopedic association) annual meeting, Victoria BC, June 2018, Canada. Oral Presentation: “The Influence of Surgical Approach on Acetabular Component Positioning: A Comparative Study of Patients Underwent Bilateral THA Through Different Approaches by the Same Surgeon”.

COA (Canadian Orthopedic association) annual meeting. Victoria BC, June 2018, Canada. Poster Presentation: “Safety and Effectiveness Of DAA-THA: A Decade`s Experience at a Tertiary Care Center”.

ORS (Orthopedic Research Society) Annual meeting, San Diego, March 2017, California. Oral presentation: “Grow and Differentiate Stem Cells in Macroporous Scaffolds and the Application to Cartilage Repair”.

Hans K. Uhthoff Research Day, Ottawa, May 2017, Canada. Oral presentation: “A decade’s experience with the Anterior Approach for Total Hip Replacement at a tertiary Care center”.

Asia Pacific Orthopedic Society APOA Congress, Melbourne, March 2016, Australia. Oral presentation: “Treatment of Congenital Pseudoarthrosis of Tibia and Fibula with Combined Approach of Periosteal Flap and Bone Graft”.

BMES (Biomedical Engineering Society) Annual Meeting, Minneapolis, October 2016, Minnesota. Oral presentation: “Hand-spun micro/nanofibers for cartilage regeneration”.

Mansoura International Foot and Ankle Course (MIFAC), Mansoura 2013, Egypt. Oral presentation: “Clubfeet in AMC and MMC”.

Mansoura International Foot and Ankle Course (MIFAC), Mansoura 2012, Egypt. Oral presentation: “Ponseti method for late presentation clubfeet”.

SICOT international congress, Prague 2011, Oral presentation: “The accessory soleus muscle as a cause of persistent equinus in clubfeet treated by the Ponseti method: A report of 16 cases”.

Annual scientific meeting of the Orthopedic Department, Mansoura University with the Orthopedic Department, Alexandria University, March 2007. Oral presentation: “Intertrochanteric Fracture complication”